The American Journal of Pathology, Vol. 179, No. 2, August 2011

DOI: 10.1016/j.ajpath.2011.05.006

Tumorigenesis and Neoplastic Progression

Promotion of Liver and Lung Tumorigenesis in DEN-Treated Cytoglobin-Deficient Mice

Le Thi Thanh Thuy,*† Takashi Morita,‡ Kayo Yoshida,‡ Kenichi Wakasa,§ Masashi Iizuka,*† Tomohiro Ogawa,*† Mami Mori,* Yumiko Sekiya,*† Shinobu Momen,*† Hiroyuki Motoyama,* Kazuo Ikeda,¶ Katsutoshi Yoshizato,*†‖ and Norifumi Kawada*†

From the Departments of Hepatology, Molecular Genetics,‡ and Diagnostic Pathology,§ and the Liver Research Center,† Graduate School of Medicine, Osaka City University, Osaka; the Department of Anatomy and Cell Biology,¶ Graduate School of Medical Sciences, Nagoya City University, Aichi; and the Academic Advisor's Office,‖ PhoenixBio Co., Ltd., Hiroshima, Japan*

Cytoglobin (Cygb) is a recently discovered vertebrate globin with molecular characteristics that are similar to myoglobin. To study the biological function of Cygb *in vivo*, we generated *Cygb* knockout mice and investigated their susceptibility to *N*,*N*-diethylnitrosamine (DEN)–induced tumorigenesis. Four-week-old male mice were administered DEN in drinking water at a dose of 25 ppm for 25 weeks or 0.05 ppm for 36 weeks. *Cygb* deficiency promoted the DEN-induced development of liver and lung tumors. All $Cygb^{+/-}$ and $Cygb^{-/-}$ mice treated with 25-ppm DEN exhibited liver tumors, compared with 44.4% of their wild-type counterparts. Lung tumors were present only in *Cygb*-deficient mice. More than 40% of $Cygb^{-/-}$ mice developed liver and lung tumors at the nontoxic dose of DEN (0.05 ppm), which did not induce tumors in wild-type mice. *Cygb* loss was associated with increased cancer cell proliferation, elevated extracellular signal–regulated kinase and Akt activation, overexpression of IL-1β, IL-6, Tnfα, and Tgfβ3 mRNAs, and hepatic collagen accumulation. *Cygb*-deficient mice also exhibited increased nitrotyrosine formation and dysregulated expression of cancer-related genes (cyclin D2, p53, Pak1, Src, Cdkn2a, and Cebpa). These results suggest that *Cygb* deficiency induces susceptibility to cancer development in the liver and lungs of mice exposed to DEN. Thus, globins such as Cygb will shed new light on the biological features of organ carcinogenesis. *(Am J Pathol 2011, 179:1050–1060; DOI: 10.1016/j.ajpath.2011.05.006)*

Cytoglobin (Cygb) was originally identified in 2001 as a protein up-regulated in rat hepatic stellate cells under profibrotic conditions. Accordingly, Cygb was originally termed a stellate cell activation-associated protein[1] until it was identified as the fourth globin in mammals.[2,3] Human Cygb displays approximately 25% amino acid identity with vertebrate myoglobin and hemoglobin and 16% identity with human neuroglobin. The *Cygb* gene is localized to chromosome 17q25.3 in humans and chromosome 11E2 in mice.

Unlike myoglobin, which is tissue restricted to cardiomyocytes and skeletal myofibers, hemoglobin in erythrocytes, and neuroglobin in the nervous system, Cygb is ubiquitously expressed in the cytoplasm of mesenchymal fibroblastic cells in many organs, including the heart, lung, liver, kidneys, small intestine, and spleen. The presence of Cygb in the nucleus of these cells has also been reported.[4,5] In particular, Cygb was present in stellate cells and myofibroblasts in the liver and pancreas, reticulocytes in the spleen, mesenchymal cells in the submucosal layer of the gut, and the mesangium and stromal cells of the kidney.[4] An interesting aspect of Cygb expression is its presence in visceral cells, with a strong storage ability for vitamin A. Thus, Cygb may facilitate the diffusion of oxygen through tissues, scavenge nitric oxide (NO) or other reactive oxygen species, or serve a protective function during oxidative stress.[6] However, the precise physiological role of Cygb *in vivo* remains unresolved. Cygb is considered a hypoxia-responsive molecule because its mRNA expression is augmented under hypoxia in fibroblastic cell lineages and rat brain.[7] Hypoxia-inducible factor 1 is assumed to be an important transcription factor for *Cygb* because hypoxia-responsive elements at positions -141, -144, and -448 are essential for the acti-

Supported by a Grant-in-Aid for Scientific Research from the Japan Society for the Promotion of Science [grant 21390232 (2009) to N.K.]; grants from the Ministry of Health, Labour, and Welfare of Japan (2008); and the Thrust Area Research grant from Osaka City University (2008).

Accepted for publication May 2, 2011.

Presented in part at the 16th International Symposium on Cells of the Hepatic Sinusoid, Pasadena, CA, September 2, 2010.

Address reprint requests to Norifumi Kawada, M.D., Ph.D., Department of Hepatology, Graduate School of Medicine, Osaka City University, 1-4-3 Asahimachi, Abeno, Osaka 545-8585, Japan. E-mail: kawadanori@med.osaka-cu.ac.jp.

vation of CYGB gene expression, and the binding of hypoxia-inducible factor 1 to this area has been confirmed.[8,9] In contrast, CYGB overexpression rescues the human neuronal cell line TE671 from prooxidant Ro19-8022–induced DNA damage.[10] CYGB overexpression also protected human neuroblastoma SH-SY5Y cells from H_2O_2-induced cell death.[11,12] Furthermore, the *in vitro* and *in vivo* overexpression of Cygb in rat hepatic stellate cells protected these cells against oxidative stress and inhibited their differentiation into an active phenotype.[13] Together, these reports suggest that Cygb may act as a cytoprotective and radical-scavenging molecule in addition to its function as a gas carrier.

Although the function of Cygb *in vivo* remains largely unknown, down-regulation of CYGB has been reported in several human cancerous tissues and human cancer cell lines. Decreased expression of CYGB and the hypermethylation of the CYGB promoter has been reported in patients with tylosis, non–small-cell lung carcinoma tissues, head and neck cancers, ovarian cancers, and breast cancers.[14–18] McRonald et al[14] reported that CYGB gene expression in tylosis with esophagus cancer was reduced to approximately 70% compared with the normal esophagus and was accompanied by hypermethylation of the promoter. Xinarianos et al[15] reported a significant reduction of CYGB mRNA expression in non-small-cell lung carcinoma tissues and hypermethylation of CYGB, compared with healthy samples. Similar results were reported in head and neck, ovarian, and breast cancer tissues.[16–18] In addition, Shivapurkar et al[19] reported high levels of CYGB promoter methylation in lung, breast, bladder, and colon cancers and in leukemia in humans. The augmented growth of NCI-H661 lung cancer cells that were CYGB silenced by RNA interference and the suppression of NCI-H228 cell proliferation in cells stably transfected with plasmids containing CYGB cDNA have also been reported.[19] These reports indicate a tumor suppressor function of *Cygb*.

To study the biological function of *Cygb* at the tissue level, we first generated *Cygb*-deficient ($Cygb^{-/-}$) mice and observed that, after treatment with *N,N*-diethylnitrosamine (DEN), $Cygb^{-/-}$ mice showed a high incidence of tumor development in the liver and lungs. These results indicate the tumor suppressor role of *Cygb in vivo*.

Materials and Methods

Materials

All experimental reagents were obtained from Sigma Chemical Co (St. Louis, MO) or Wako Pure Chemical Co (Osaka, Japan), unless otherwise stated.

Construction of the Targeting Vector

Mice lacking exon 1 of the *Cygb* gene were generated using the lox-P system, as previously described.[20] The targeting vector (pTVneo/*Cygb*) was constructed from PCR DNA fragments from 129Sv mouse genomic DNA. Two DNA fragments were used as the 3′ and 5′ arms. One fragment contained *Cygb* exons 2, 3, and 4 (6.5 kb); and the other contained the transcription initiation site in exon 1 and the 5′ upstream sequence of the *Cygb* gene (6.0 kb). The neomycin-resistance gene, driven by the phosphoglycerate kinase 1 promoter, flanking the lox-P sequences was inserted into the arms (Figure 1A).

Embryonic stem cells (1×10^7 cells/mL) were transfected with a linearized targeting vector (20 μg) by electroporation and cultured in selection medium containing 150 μg/mL geneticine (G418). Of 480 neomycin-resistant clones, 6 (1.2%) were homologous recombinants by Southern blotting using the 5′ probe (data not shown).

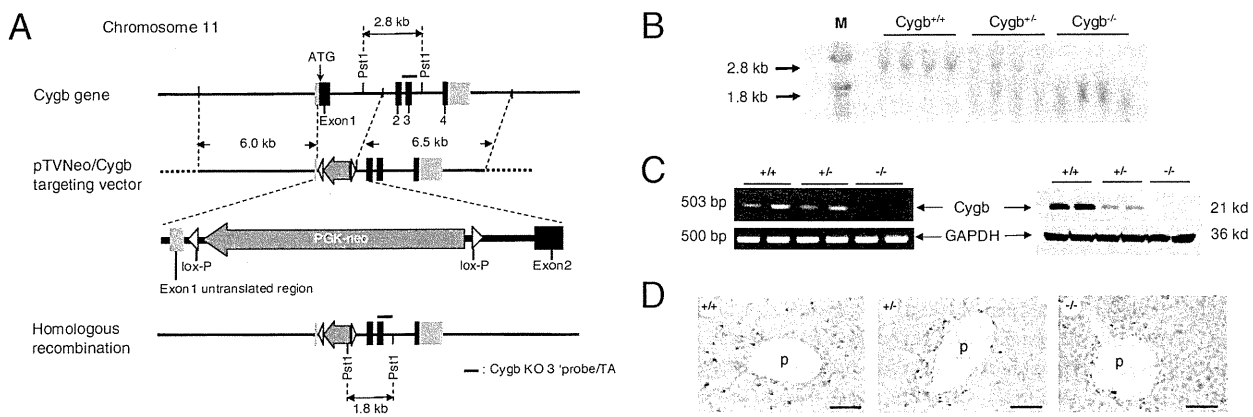

Figure 1. Generation of *Cygb*-deficient mice. **A:** Strategy for inactivation of the *Cygb* gene by homologous recombination in embryonic stem cells. A partial genomic map of the *Cygb* gene with coding exons (**black boxes**), noncoding regions (**light gray boxes**), and flanking introns (**solid lines**) is shown (**top**). Targeting vector pTVneo/*Cygb* with homology to the *Cygb* gene locus is shown (**middle**). The translation initiation site in exon 1 was replaced with a neomycin-resistance cassette. The predicted *Cygb* gene locus after homologous recombination is shown (**bottom**). **B:** Southern blot analysis shows the sizes of the wild-type (2.8-kb) and disrupted (1.8-kb) *Cygb* fragments after PstI cleavage. M, molecular weight marker. **C:** RT-PCR and immunoblot analysis of Cygb expression in the liver from $Cygb^{+/+}$, $Cygb^{+/-}$, and $Cygb^{-/-}$ mice. GAPDH was used as a loading control. **D:** Representative IHC images of Cygb in the liver of $Cygb^{+/+}$, $Cygb^{+/-}$, and $Cygb^{-/-}$ mice. Cygb is present along the sinusoids of $Cygb^{+/+}$ mice, whereas it is undetectable in $Cygb^{-/-}$ mice. p, portal vein. Scale bar = 50 μm.

Production of Cygb-*Deficient Mice*

Two clones were aggregated with C57BL/6-DBA2 F1 mouse morulae, and one produced chimeric mice that transmitted the knockout (KO) construct. Chimeric males were mated with C57BL/6J females to obtain *Cygb* heterozygous mice that were backcrossed to the C57BL/6J background for more than nine generations. To assess the role of the *Cygb* gene in development, we intercrossed *Cygb* heterozygous mice. The litter sizes were normal, and analysis of the tail biopsy specimens at the age of 4 weeks, from 102 offspring from heterozygote crosses, revealed the presence of homozygous mutant mice at a frequency of 24%. The homozygotes appeared normal morphologically and histopathologically 1 month after birth. Four-week-old $Cygb^{+/+}$ (wild-type), $Cygb^{+/-}$ (heterozygote), and $Cygb^{-/-}$ (homozygote) male mice were used in this study.

All mice were cared for according to the guidelines approved by the Institutional Animal Care and Use Committee of Osaka City University, Osaka.

Genotyping of Mice

PCR genotyping of mouse tail DNA produced the expected 338-bp product from wild-type mice using the following primer pairs: forward, 5′-CTCCCAGCCGGGACCGCG-GTGGCCTT-3′; and reverse, 5′-GGAGCCGAGGCCGGT-GCGTGCGAGGC-3′. A 529-bp product was diagnostic for the *Cygb* KO allele using the described forward primer and the following reverse primer: 5′-GTGGGGTGGGATT-AGATAAATGCCTGCTCT-3′. PCR was performed in a 15-μL reaction mixture containing 1 μL of extract from mouse tail DNA, which was digestion extracted using LYPPO (Gene Modification R&D Co Ltd, Osaka), according to the manufacturer's protocol; 1 μmol/L of each primer; 2.5% to 5% dimethyl sulfoxide; and 0.5 U GO Taq polymerase (Promega, San Luis Obispo, CA). PCRs were performed for 40 cycles, each cycle being 1 minute at 94°C, 30 seconds at 70°C, and 1 minute at 72°C.

Southern blot analysis confirmed the *Cygb*-null allele. Genomic tail DNA (5 μg) was cleaved with PstI, subjected to agarose gel electrophoresis, blotted onto nylon membranes, and hybridized to the ^{32}P-labeled *Cygb* KO 3′ probe/TA (Figure 1A). DNA fragments of 2.8 and 1.8 kb represented the *Cygb* wild-type and null alleles, respectively.

RT-PCR was performed to confirm the absence of Cygb mRNA in tissues. Total RNA was extracted from the homogenates of liver tissues using the RNeasy Mini Kit (Qiagen, Valencia, CA). cDNA was synthesized using 1 μg of total RNA, ReverTra Ace (Toyobo, Osaka), and oligo $(dT)_{12-18}$ primers, according to the manufacturer's instructions. Thirty-five PCR cycles (30 seconds at 94°C, 30 seconds at 68°C, and 1 minute at 72°C) were run using the following mouse Cygb primers: forward, 5′-GCGACATGGAGATAGAGCGT-3′; and reverse, 5′-CTG-TACCCAGCCCACTTCCT-3′. This generated a 503-bp product and glyceraldehyde-3-phosphate dehydrogenase (GAPDH) primers: forward, 5′-CGCCTGGTCAC-CAGG-3′; and reverse, 5′-CAGTTGGTGGTGCAGGA-3′). A 500-bp product was generated.

Administration of DEN

DEN (0.95 g/mL) was obtained from Sigma Chemical Co. A stock solution of DEN was prepared by dissolving 1 g (1.06 mL) of DEN in 400 mL of water. The stock solution was diluted 100-fold before use to obtain a final concentration of 25-mg DEN per 1000-mL water (25 ppm) for the high-dose experiment. The 25-ppm solution was further diluted 500-fold to obtain a final concentration of 0.05-mg DEN per 1000-mL water (0.05 ppm) for the low-dose experiment. The diluted solution (25 or 0.05 ppm) was placed in a shaded serving bottle and administered to the animals instead of water. The diluted solution was prepared weekly. The administration of DEN to male mice began at the age of 4 weeks for 25 weeks in the high-dose experiment (25 ppm) and for 36 weeks in the low-dose experiment (0.05 ppm). Each experiment contained three groups ($Cygb^{+/+}$, $Cygb^{+/-}$, and $Cygb^{-/-}$) with a

Table 1. Primary Antibodies Used for IHC Analyses

Antigen*	Source	Name/clone; catalog no.	Incubation
AFP	US Biological, Swampscott, MA	F4100-16A (Go)	Overnight 4°C, 1:20
CK19	Santa Cruz Biotechnology, Santa Cruz, CA	Polyclonal (Rb); sc-33111	Overnight 4°C, 1:100
CRBP-1	Santa Cruz Biotechnology	Polyclonal (Rb); sc-30106	Overnight 4°C, 1:100
Cygb	Our laboratory†	Polyclonal (Rb)	Overnight 4°C, 1:100
Erk	Cell Signaling, Danvers, MA	Monoclonal (Rb); 4695	Overnight 4°C, 1:300
PCNA	Dako, Glostrup, Denmark	Monoclonal (Mo)‡; clone: PC-10	Overnight 4°C, 1:200
Phosphorylated Erk	Cell Signaling	Monoclonal (Rb); 4370	Overnight 4°C, 1:200
α-SMA	Dako	Monoclonal (Mo)‡; clone: 1A4	30 minutes at room temperature, 1:100
Desmin	Santa Cruz Biotechnology	Polyclonal (Go); sc-7559	Overnight 4°C, 1:100

*All antigens were retrieved by autoclaving for 15 minutes in 0.01 mol/L citrate buffer containing 0.05% Tween 20 (pH 6.0), except for desmin, which was used in Tris-EDTA buffer (pH 9.0).

†Data taken from Kawada et al.[1]

‡For mouse primary antibodies, after antigen retrieval, sections were incubated with goat anti-mouse IgG Fab fragments (Jackson ImmunoResearch Laboratories) for 1 hour at room temperature (1:100) to block nonspecific background staining.

AFP, alpha-fetoprotein.

minimum of seven mice per group. Mice were sacrificed after the completion of DEN treatment.

Necropsy

At necropsy, mice were weighed, anesthetized, and examined for grossly visible lesions in whole organs. Livers and lungs were excised, weighed (in the case of liver), and examined for macroscopic lesions. The number of macroscopic abnormal masses ≥1 mm was determined in addition to the size of the mass by taking the average of the largest and smallest length of the mass. For histological examination, 2- to 3-mm-thick sections from nontumor or tumor tissues were fixed in 10% formalin for 24 hours and embedded in paraffin. The samples were then sectioned at 5 μm and stained with H&E.

IHC and TUNEL Assays

For immunohistochemistry (IHC), paraffin sections were dewaxed in xylene and rehydrated in decreasing concentrations of ethanol. The primary antibodies and conditions used for IHC are listed in Table 1. Negative controls with no primary antibody were used to assess nonspecific staining. The secondary antibodies used were horseradish peroxidase–conjugated goat anti-rabbit IgG (1:200; Dako, Glostrup, Denmark), rabbit anti-goat IgG (1:200; Dako), or rabbit anti-mouse IgG (1:200; Dako). 3,3′-Diaminobenzidine (Dako) was used as the chromogen. TdT-mediated dUTP-biotin nick-end labeling (TUNEL) staining was performed using the *In situ* Apoptosis Detection Kit (MK500; TaKaRa Bio Inc., Shiga, Japan), according to the manufacturer's protocol. All sections were counterstained with Meyer's hematoxylin.

Quantification of Liver Fibrosis

Morphometric image analysis was performed in liver tissue specimens with a computerized system, consisting of a photomicroscope, a digital camera, and LuminaVision 2.4 bioimaging software (Mitani Corporation, Tokyo, Japan) to quantitatively assess fibrosis. The proportion of the area stained with Sirius red in the liver sections was calculated as the sum of the pixelwise-bound stain measurements divided by the number of summed pixels.

Quantitative Real-Time PCR

Total RNA was extracted from liver and liver tumor tissues using the RNeasy Mini Kit (Qiagen, Valencia, CA). cDNAs were synthesized as previously described. Gene expression was measured by quantitative real-time PCR using cDNA, real-time PCR Master Mix Reagents (Toyobo, Osaka), or TaqMan Fast Universal PCR Master Mix (Applied Biosystems, Foster City, CA), and a set of gene-specific oligonucleotide primers and probes (Table 2) using an Applied Biosystems Prism 7500 (Applied Biosystems). GAPDH levels were measured and used to normalize the relative abundance of mRNA.

Table 2. Primers Used for RT-qPCR

Gene	Sequence
AFP	
Forward	5′-CACACCCGCTTCCCTCAT-3′
Reverse	5′-TTTTCGTGCAATGCTTTGGA-3′
Bcl2	
Forward	5′-AAGGGCTTCACACCCAAATCT-3′
Reverse	5′-CTTCTACGTCTGCTTGGCTTTGA-3′
Cdkn2a	
Forward	5′-GCTCTGGCTTTCGTGAACATG-3′
Reverse	5′-GTGCGGCCCTCTTCTCAA-3′
Cebpα	
Forward	5′-CGCAAGAGCCGAGATAAAGC-3′
Reverse	5′-CGGTCATTGTCACTGGTCAACT-3′
Col1α1	
Forward	5′-GACATCCCTGAAGTCAGCTGC-3′
Reverse	5′-TCCCTTGGGTCCCTCGAC-3′
Cyclin D1	
Forward	5′-GCCCGGAGGGATTTGC-3′
Reverse	5′-AGACGGAACACTAGAACCTAACAGATT-3′
Cyclin D2	
Forward	5′-AAGGCAGATACTCATCAAACACAGA-3′
Reverse	5′-CTGGTGCACGCATGCAA-3′
Fos	
Forward	5′-CCCCAAACTTCGACCATGAT-3′
Reverse	5′-GGAGGATGACGCCTCGTAGTC-3′
GAPDH	
Forward	5′-TGCACCACCAACTGCTTAG-3′
Reverse	5′-GGATGCAGGGATGATGTTC-3′
IL-6	
Forward	5′-CGCTATGAAGTTCCTCTCTGCAA-3′
Reverse	5′-CACCAGCATCAGTCCCAAGA-3′
IL-1β	
Forward	5′-CCATGGCACATTCTGTTCAAA-3′
Reverse	5′-GCCCATCAGAGGCAAGGA-3′
Jun	
Forward	5′-CCGCCCCTGTCCCCTAT-3′
Reverse	5′-TCCTCATGCGCTTCCTCTCT-3′
Pak1	
Forward	5′-CGTATTGCGGGTGTTTGCTA-3′
Reverse	5′-CACAGCAGGAGAACCAAAACC-3′
p53	
Forward	5′-GCATGAACCGCCGACCTAT-3′
Reverse	5′-CAGAAGGTTCCCACTGGAGTCT-3′
Src	
Forward	5′-CCTCCCGCACCCAGTTC-3′
Reverse	5′-CATCAGCATGTTTGGAGTAGTAAGC-3′
TGFβ3	
Forward	5′-AGGGCCCTGGACACCAATTAC-3′
Reverse	5′-CCTTAGGTTCTGGGACCCATTTC-3′
TNFα	
Forward	5′-CCTCACACTCAGATCTTCTCA-3′
Reverse	5′-GCTGCTCCTCCACTTGGTG-3′
Probe	5′-GCAAGCCTGTAGCCCACGTCGTAGCAAA-3′

Immunoblotting

Protein samples (10 to 20 μg) were subjected to SDS-PAGE and transferred to Immobilon P membranes (Millipore Corp, Bedford, MA). After blocking, membranes were probed with primary antibodies against Cygb (1:500) from our laboratory (Table 1), Akt (1:1000; Cell Signaling, Danvers, MA), phosphorylated Akt (1:500; Cell Signaling), extracellular signal–regulated kinase (Erk; 1:500; Cell Signaling), phosphorylated Erk (1:1000; Cell Signaling), cyclin D1 (1:5000; Cell Signaling), nitrotyrosine (1:500; Cell Signaling), or GAPDH (1:2000; Santa Cruz Biotechnology, Santa Cruz, CA). Membranes were

then labeled with horseradish peroxidase–conjugated secondary antibodies. Immunoreactive bands were visualized using the ECL detecting reagent (GE Healthcare UK Ltd, Buckinghamshire, UK) and documented with an LAS 1000 (Fuji Photo Film, Kanagawa, Japan).

Data Analyses

The data presented as bar graphs are the means ± SDs in all experiments. Statistical analyses were performed using the Student's *t*-test, and $P < 0.05$ indicated statistical significance.

Results

Characterization of the Cygb$^{-/-}$ *Mice*

Cygb-deficient mice were generated by deleting exon 1 of the mouse *Cygb* gene (Figure 1A) and backcrossed on the C57BL/6J background. Southern blotting (Figure 1B) and PCR genotyping using mouse tail DNA (data not shown) confirmed the deletion of the *Cygb* gene. Both Cygb mRNA and protein expression were absent in *Cygb*$^{-/-}$ mouse livers, compared with wild-type livers (Figure 1C). Furthermore, IHC indicated that the Cygb protein was present in sinusoidal lining cells in addition to perivascular cells around the portal and central veins, as previously reported,[1] in *Cygb*$^{+/+}$ mice, whereas it was undetected in *Cygb*$^{-/-}$ mice (Figure 1D). Together, these data demonstrate the successful production of the *Cygb*$^{-/-}$ mice.

The mice homozygous for the disrupted allele appeared normal both morphologically and histopathologically 1 month after birth. Next, we examined whether Cygb influenced the toxicity and carcinogenesis of DEN in mice.

Cygb Deficiency Strongly Promotes DEN-Induced Tumorigenesis

DEN is a commonly used chemical carcinogen for the liver because it is activated by cytochrome P-450 enzymes in hepatocytes.[21] C57BL/6J mice were reported to be relatively resistant to liver tumor development under DEN treat-

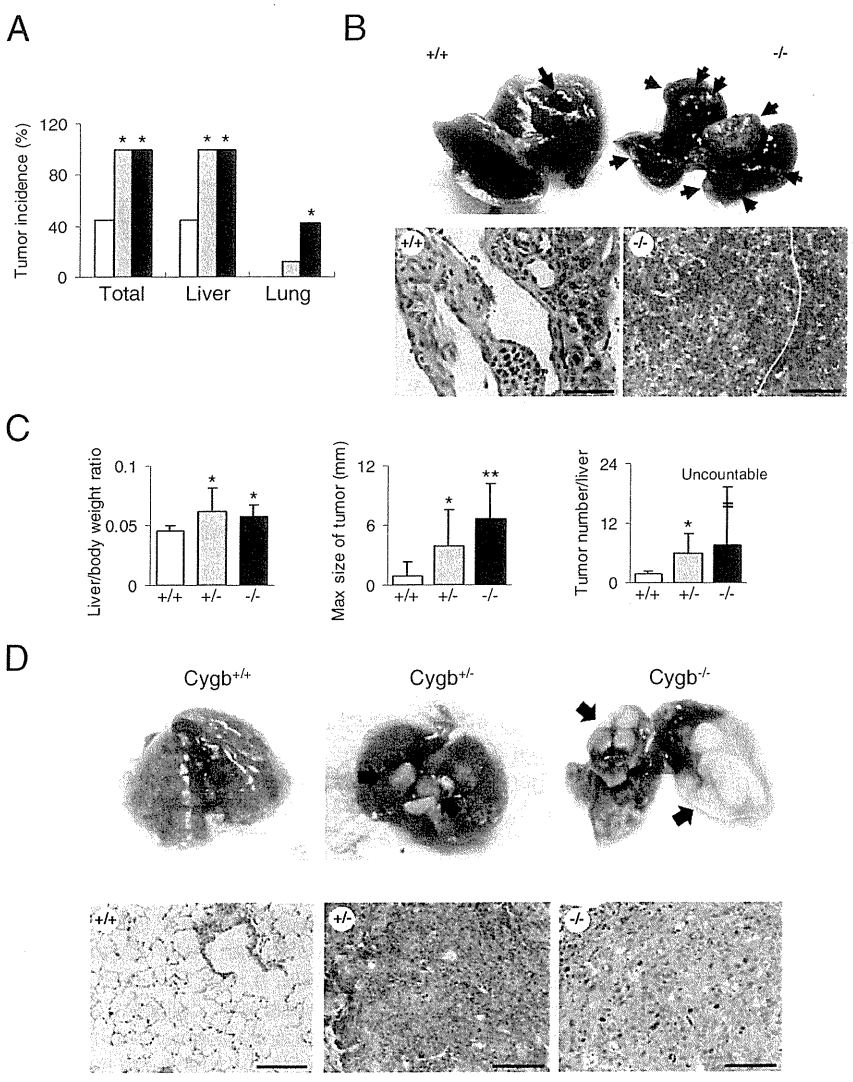

Figure 2. Tumor development in *Cygb*-deficient mice treated with 25-ppm DEN for 25 weeks. **A:** Tumor incidence in total, livers, and lungs from DEN-treated *Cygb*$^{+/+}$ (white bars), *Cygb*$^{+/-}$ (gray bars), and *Cygb*$^{-/-}$ (black bars) mice (n = 7 to 12). $^{*}P < 0.05$ compared with wild type. **B:** Representative gross photographs of livers (**top**) from wild-type (+/+) and *Cygb*-KO (−/−) mice treated with DEN. There was a marked increase in tumor multiplicity in *Cygb*-deficient mice compared with wild-type mice (**arrows**). Representative H&E-stained paraffin sections (**bottom**) of hemangioma from wild-type and poorly differentiated hepatocellular carcinoma composed of small immature neoplastic cells with mitotic figures (the line indicates the boundary of tumor and nontumor areas), from *Cygb*$^{-/-}$ mice. Scale bar = 100 μm. **C:** Determination of liver/body weight ratios, maximum (Max) tumor sizes, and liver tumor numbers for *Cygb*$^{+/+}$ (white bars), *Cygb*$^{+/-}$ (gray bars), and *Cygb*$^{-/-}$ (black bars) mice (n = 7 to 12). Values are given as the mean ± SD. $^{*}P < 0.05$, $^{**}P < 0.01$. **D:** Representative gross photographs (**top**) and microphotographs (**bottom**) of lungs from *Cygb*$^{+/+}$, *Cygb*$^{+/-}$, and *Cygb*$^{-/-}$ DEN-treated mice. Lung tumors were only found in *Cygb*$^{+/-}$ and *Cygb*$^{-/-}$ mice. **Arrows** indicate lung tumors that were classified as squamous cell carcinomas. Scale bar = 100 μm.

ment.[22,23] In this study, we examined whether the loss of Cygb could influence the toxicity and carcinogenesis of DEN in the tumor-resistant C57BL/6J strain. We administered 25-ppm DEN to the drinking water of *Cygb*-deficient male mice at the age of 4 weeks. Unexpectedly, as early as 25 weeks after DEN treatment, 100% of $Cygb^{-/-}$ and $Cygb^{+/-}$ mice developed tumors in the liver and lungs, whereas the tumor incidence in wild-type mice was 44.4% (Figure 2, A and B). The liver/body weight ratio was approximately 50% more than in wild-type animals (Figure 2C) because of these tumor masses. $Cygb^{-/-}$ mice displayed significantly larger lesions and produced tumors more frequently than wild-type mice (Figure 2C).

DEN has induced tumors in the liver and in the lungs of the B6C3F1 mouse strain, although with a lower frequency.[24] Consistent with these studies, lung tumors were found in $Cygb^{+/-}$ and $Cygb^{-/-}$ mice, with a frequency of 11.7% and 57.1%, respectively, whereas $Cygb^{+/+}$ mice showed complete resistance (Figure 2, A and D).

Next, using a low dose of DEN, at which wild-type mice do not develop liver tumors, we examined whether *Cygb* deficiency functioned as a tumor promoter. We took advantage of earlier observations that, when DEN was administered to mice at a nontoxic dose, it failed to induce liver cancer, unless combined with a tumor promoter, such as phenobarbital.[25,26] We maintained wild-type and *Cygb*-deficient male mice during DEN administration at the nontoxic dose of 0.05 ppm for 36 weeks. As a result, >40% of $Cygb^{-/-}$ mice developed tumors in the liver or lungs, whereas, as expected, wild-type mice exhibited no tumor formation (Figure 3). $Cygb^{+/-}$ mice showed an intermediate sensitivity. These findings confirm the tumor-promoting effects of *Cygb* depletion.

To define the histological features of the liver tumors, liver samples were evaluated IHC. The liver tumors in C57BL/6 mice (wild type) administered DEN in drinking water were dominantly composed of cholangiomas, hemangiomas, hemangiosarcomas, and, to a lesser degree, hepatocellular carcinomas.[27–29] In this study, *Cygb*-deficient and wild-type mice developed similar histological alterations in the liver, including hemangioma (Figure 2B), hepatocellular carcinoma (Figures 2B and 3B), which stained positive for alpha-fetoprotein (AFP) (Figure 4A), and cholangioma, which stained positive for CK19 (Figure 4A). Quantitative real-time PCR (RT-qPCR) analysis showed increased mRNA expression of AFP in $Cygb^{+/-}$ and $Cygb^{-/-}$ mice compared with their wild-type counterparts (Figure 4B).

In the liver, Cygb was present in stellate cells.[1,4] We used cellular retinol-binding protein-1 and α-smooth muscle actin antibodies to detect stellate cell expression. The presence of cellular retinol-binding protein-1– and α-smooth muscle actin–expressing cells in the liver parenchyma from DEN-treated homozygote mice indicated that stellate cells were present along sinusoids, even in the absence of Cygb (Figure 4C). The expression of α-smooth muscle actin and desmin, another marker of stellate cells, was markedly augmented in $Cygb^{-/-}$ mice (Figure 4C). Next, we assessed whether liver fibrosis developed in these mice. Sirius red staining for collagen deposition in paraffin-embedded sections of liver samples

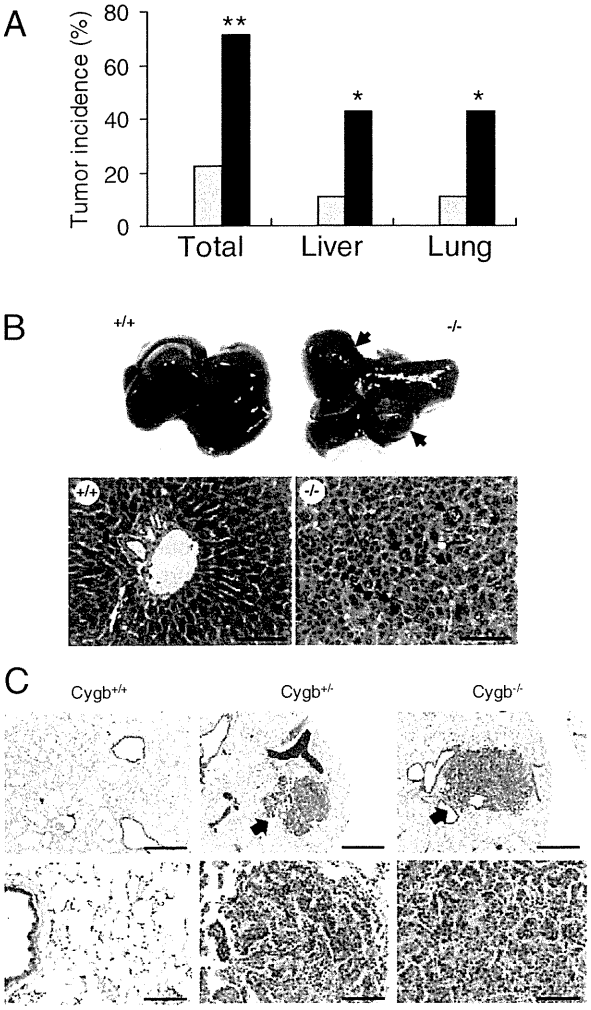

Figure 3. Tumor development in *Cygb*-deficient mice treated with 0.05-ppm DEN for 36 weeks. **A:** Tumor incidence in total, livers, and lungs from 0.05-ppm DEN-treated $Cygb^{+/+}$ (white bars), $Cygb^{+/-}$ (gray bars), and $Cygb^{-/-}$ (black bars) mice (n = 7 to 15). $^{*}P < 0.05$, $^{**}P < 0.01$ compared with the wild type. **B:** Gross photographs of livers (**top**) from $Cygb^{+/+}$ and $Cygb^{-/-}$ mice treated with 0.05-ppm DEN, as previously mentioned; **arrows** indicate lung tumors. Representative photomicrographs of H&E-stained paraffin sections of liver parenchyma (**bottom**) from wild-type and moderately differentiated hepatocellular carcinoma composed of large cells that vary in size and shape (**arrows**), from $Cygb^{-/-}$ mice. Scale bar = 100 μm. **C:** Representative photomicrographs of H&E-stained paraffin sections of lungs from $Cygb^{+/+}$, $Cygb^{+/-}$, and $Cygb^{-/-}$ mice treated with 0.05-ppm DEN for 36 weeks. Scale bars: 400 μm (**top**); 100 μm (**bottom**). **Arrows** indicate lung tumors that were classified as adenocarcinomas. No lung tumor was observed in $Cygb^{+/+}$ mice.

collected from $Cygb^{+/+}$ and $Cygb^{-/-}$ mice treated with 25-ppm DEN for 25 weeks showed marked deposition of collagen (red) around the hepatocytes (pericellular fibrosis) in $Cygb^{-/-}$ mice (Figure 4D). Morphometric image analysis was performed with a computerized system, consisting of a photomicroscope, a digital camera, and LuminaVision 2.4 bioimaging software, to quantitatively assess fibrosis. The Sirius red–positive area of $Cygb^{-/-}$ mice (7.67% ± 7.82%, n = 3) was significantly greater than that in $Cygb^{+/+}$ mice (mean ± SD, 1.36% ± 0.36%, n = 3; $P < 0.05$, Kruskal-Wallis test). Pericellular fibrosis with collagen deposition was accompanied by significantly augmented mRNA expression of collagen 1α1 and tissue inhibitor of matrix met-

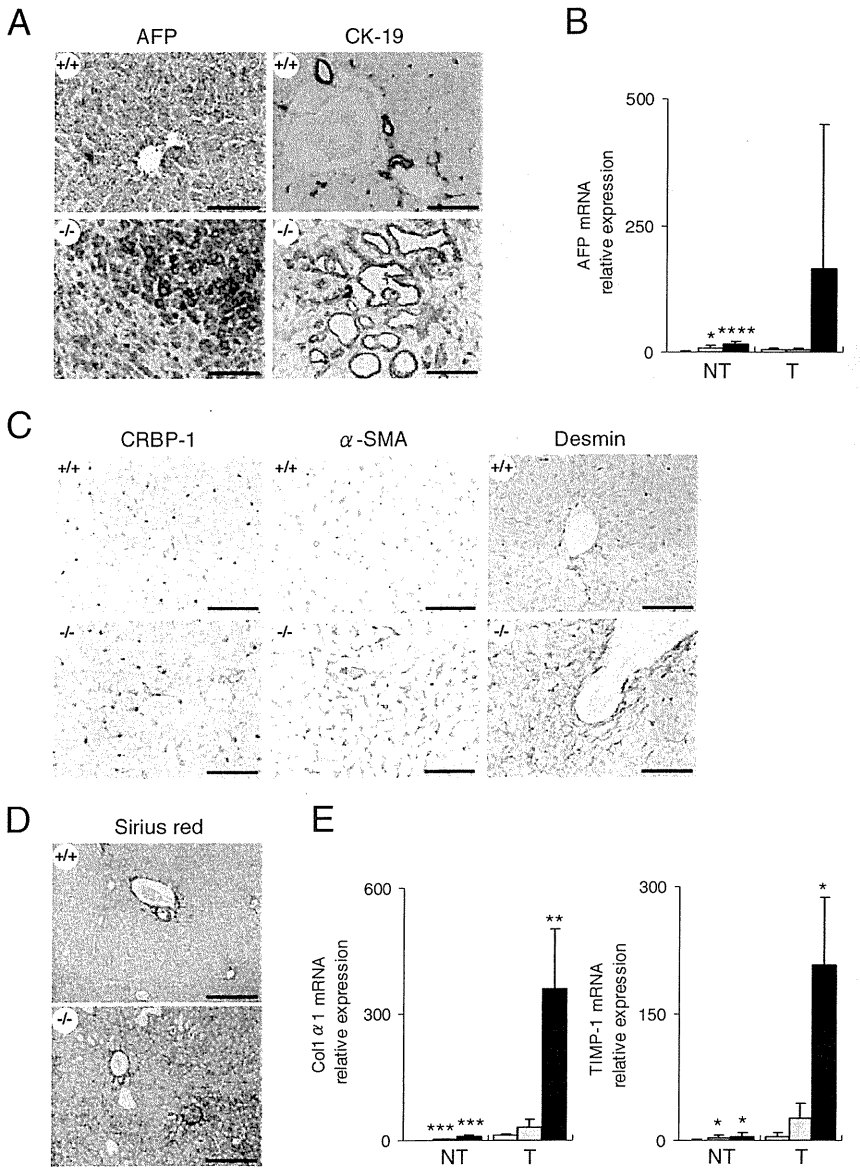

Figure 4. Expression of tumor markers and liver fibrosis development in DEN-treated *Cygb*-deficient mice. *Cygb*-deficient mice from Figure 2 were subjected to histological and biochemical analyses. **A:** Paraffin-embedded liver sections from $Cygb^{+/+}$ and $Cygb^{-/-}$ mice were stained with AFP and cytokeratin 19 (CK-19). Scale bar = 100 μm. **B:** Expression of AFP mRNA in $Cygb^{+/+}$ (white bars), $Cygb^{+/-}$ (gray bars), and $Cygb^{-/-}$ (black bars) mice livers was determined by RT-qPCR (n = 7 to 12). Levels were normalized to GAPDH. Values are given as the mean ± SD of all experiments. NT, nontumor area; T, liver tumor. $^{*}P < 0.05$, $^{****}P < 0.0001$. **C:** Paraffin-embedded liver sections were IHC stained for the detection of CRBP-1, α-SMA, and desmin. Scale bar = 100 μm. **D** and **E:** Development of liver fibrosis. **D:** Sirius red staining for collagen deposition in paraffin-embedded liver sections. Scale bar = 100 μm. There was marked deposition of collagen (red) around the hepatocytes (pericellular fibrosis) in $Cygb^{-/-}$ mice. **E:** Relative levels of collagen (Col) 1α1 and tissue inhibitor of matrix metalloproteinase-1 (TIMP-1) mRNA in the nontumor area (NT; n = 7 to 12) and in liver tumors (T; n = 3 to 5) of $Cygb^{+/+}$ (white bars), $Cygb^{+/-}$ (gray bars), and $Cygb^{-/-}$ (black bars) mice were determined by RT-qPCR and normalized to GAPDH mRNA. Values are given as the mean ± SD of all experiments. $^{*}P < 0.05$, $^{**}P < 0.01$, and $^{***}P < 0.001$.

taloproteinase-1 in the livers of $Cygb^{-/-}$ mice, compared with that of $Cygb^{+/+}$ mice treated with 25-ppm DEN for 25 weeks (Figure 4E). Thus, the augmented occurrence of pericellular fibrosis and fibrotic reactions in *Cygb* deficiency may be involved in the development of liver cancer.

Cygb *Loss Is Associated with Increased Cancer Cell Proliferation*

Two important cellular processes in tumorigenesis are cell apoptosis and proliferation. To examine how *Cygb* loss affected these two processes in the livers of C57BL/6J mice, we determined the labeling indexes of TUNEL, as a marker of apoptotic cells, and proliferating cell nuclear antigen (PCNA), as a marker of proliferating cells in the liver, both in the tumor and adjacent nontumor areas of $Cygb^{+/+}$ and $Cygb^{-/-}$ mice treated with 25-ppm DEN in drinking water for 25 weeks. Liver tumors in $Cygb^{-/-}$ mice exhibited reduced apoptotic cell death relative to liver tumors in $Cygb^{+/+}$ mice (Figure 5, A and C) and showed elevated mRNA expression of the antiapoptotic protein Bcl-2 (Figure 5E). Liver tumors in the $Cygb^{-/-}$ mice exhibited more proliferating cells than the tumors of the wild-type mice, as shown by PCNA labeling (Figure 5, B and D), in addition to elevated cyclin D1 mRNA expression (Figure 5F). These results suggest that stimulation of proliferating neoplastic cells is the primary cellular mechanism for increased liver tumorigenesis in *Cygb*-deficient mice.

Cygb-*Deficient Mice Exhibit Elevated Phosphorylated Akt and Erk and Liver Inflammation*

To identify the signaling pathways responsible for enhanced hepatocyte survival and proliferation, we ex-

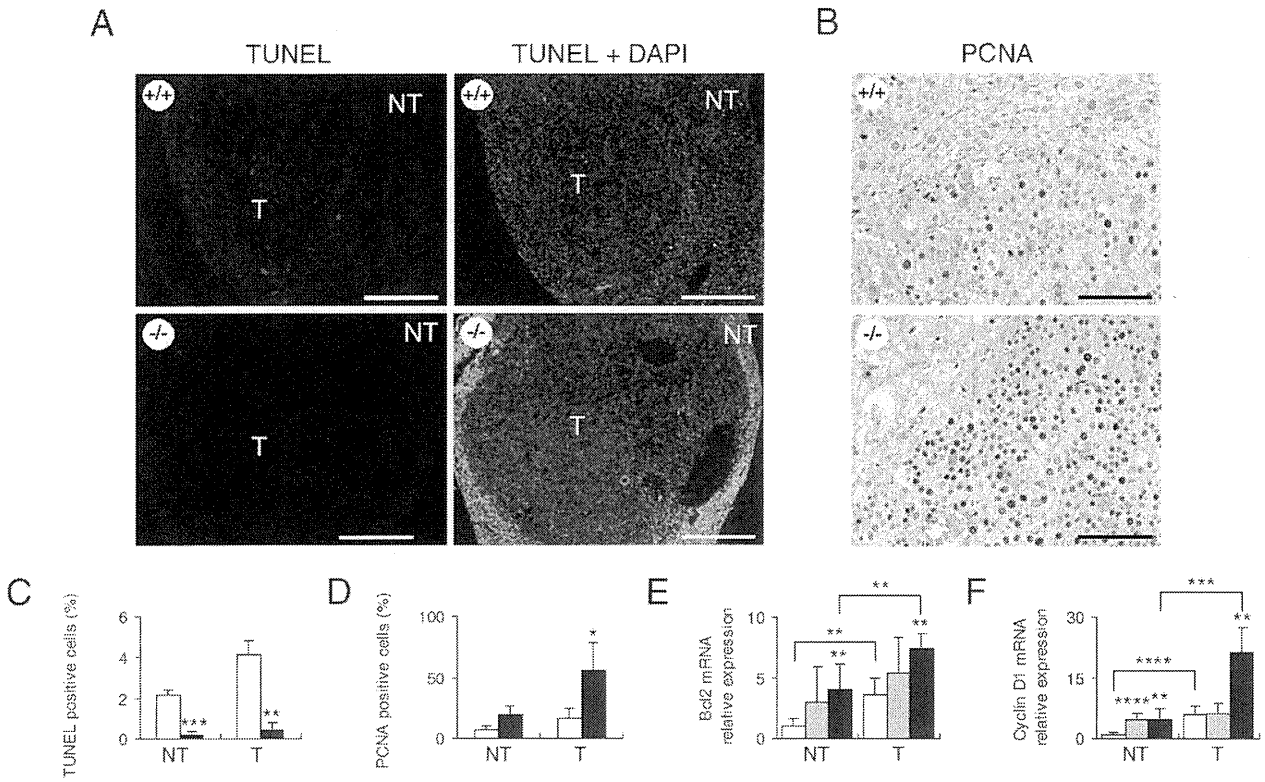

Figure 5. Tumor-bearing *Cygb*-deficient mice are associated with increased cancer cell proliferation and reduced apoptosis. **A:** Paraffin-embedded liver sections from wild-type (+/+) and homozygous (−/−) mice treated with 25-ppm DEN for 25 weeks were TUNEL labeled (**left**) and counterstained with DAPI (**right**). Apoptotic cells were present in the tumor (T) area in wild-type mice. NT, nontumor area. Scale bar = 400 μm. **B:** Paraffin-embedded liver sections were stained with PCNA. Scale bar = 100 μm. The frequency of apoptotic (**C**) or proliferate (**D**) cells was determined by counting TUNEL- or PCNA-positive cells, respectively (cells with the nucleus stained dark brown in the case of PCNA), in at least 1000 cells from each liver ($n = 3$). Expression levels of Bcl-2 (**E**) and cyclin D1 (**F**) mRNA in the NT ($n = 7$ to 12) and T ($n = 3$ to 5) areas from 25-ppm DEN-treated mice were determined by RT-qPCR and normalized to GAPDH. $Cygb^{+/+}$ (white bars), $Cygb^{+/-}$ (gray bars), and $Cygb^{-/-}$ (black bars) mice. Values are given as the mean ± SD of all experiments. $^{*}P < 0.05$, $^{**}P < 0.01$, $^{***}P < 0.001$, and $^{****}P < 0.0001$.

amined the effects of *Cygb* deficiency on the major pathways implicated in liver cancer.[30] As expected, *Cygb* loss was associated with an increase in both Akt phosphorylation and abundance in the livers (Figure 6A). This observation was also evident for Erk signaling (Figure 6, A and B). Consistent with increased Erk phosphorylation, *Cygb*-deficient mice exhibited increased expression of cyclin D1 (Figure 6A), and Jun and Fos mRNA in nontumor and tumor areas, relative to wild type (Figure 6C). These results suggested that the Akt and Erk pathways are activated in response to *Cygb* deficiency. The increased levels of Akt and Erk activation correlated with a marked elevation of IL-6 mRNA in both nontumor and tumor areas in *Cygb*-deficient mice (Figure 6D). IL-6 is a tumor-promoting cytokine that is required for Erk activation and contributes to alterations in Akt signaling.[31] Knowing that IL-6 functions as a downstream mediator for both IL-1 and tumor necrosis factor-α,[32] we examined the expression of these two cytokines. Remarkably, IL-1β and Tnfα levels (Figure 6D) increased 10- and 30-fold, respectively, at the mRNA level in the nontumor area of the liver and increased further in the tumors, relative to wild type. *Cygb*-deficient mice also had increased expression of Tgfβ3 mRNA (Figure 6D). These data suggest that *Cygb* loss can trigger inflammation and lead to the long-term elevation of tumor-promoting cytokines, resulting in the development of tumors.

Nitrotyrosine Accumulation in the Livers of DEN-Treated Cygb*-Deficient Mice*

Long-term administration of DEN has induced the expression of the inducible isoform of NO synthase and 3-nitrotyrosine, a marker of peroxynitrite formation, in preneoplastic and neoplastic rat liver tissues.[33] In this study, we detected the overproduction of nitrotyrosine in tumor and nontumor liver tissues of *Cygb*-deficient mice, compared with wild-type mice, as shown by IHC (Figure 7A) and immunoblot analyses (Figure 7B). These results indicate the high production of NO, together with superoxide, in *Cygb*-deficient mice.

Dysregulation of Genes Associated with Cell Proliferation and Differentiation in Cygb*-Deficient Mice*

To further screen for cellular alterations caused by *Cygb* gene disruption, we compared gene expression profiles between *Cygb*-deficient mice and their wild-type counterparts after 25-ppm DEN treatment for 25 weeks. We

observed the altered expression of cancer genes, including p53, cyclin D2, Pak1 (p21-activated kinase), Src, Cdkn2a, and Cebpa (CCAAT/enhancer-binding protein α) (data not shown). We examined in detail the mRNA levels of these genes by RT-qPCR. Consistent with the high rate of cellular proliferation in the liver of *Cygb*-deficient mice (Figure 5, B and D), we observed overexpression of cyclin D2 (Figure 8A) and p53 (Figure 8B), which have displayed high expression in astrocytomas, a type of brain tumor.[34] Pak1 promotes malignant tumor progression, and the Src proto-oncogene has shown increased expression in human skin tumors and leukemia.[35–38] In this study, we found that the mRNA expression of Pak1, in addition to Src, increased fivefold in the livers of $Cygb^{-/-}$ mice, relative to the wild type (Figure 8, C and D).

Cdkn2a, a tumor suppressor that negatively regulates the cell cycle, displayed increased expression at the mRNA level in the livers of *Cygb*-deficient mice (Figure 8E), consistent with other studies[39,40] on sarcomas and lung tumors.

Cebpa has the ability to inhibit proliferation, particularly in hepatocytes.[41,42] Down-regulation of CEBPA has been reported in human myeloid leukemia.[43] Consistent with these studies, our results showed decreased expression of Cebpa mRNA in the liver of *Cygb*-deficient mice, relative to the wild type (Figure 8F).

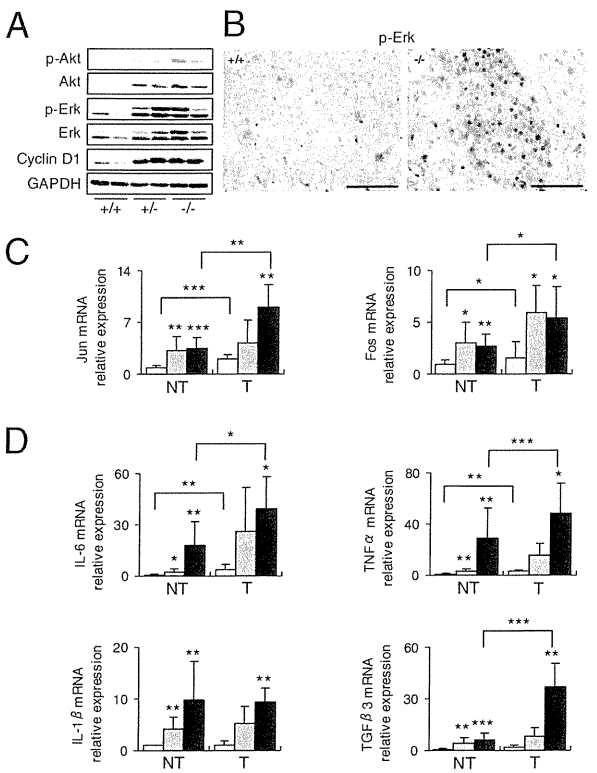

Figure 6. Tumor-bearing *Cygb*-deficient mice exhibited elevated phosphorylated Akt (p-Akt), phosphorylated Erk (p-Erk), and inflammation. *Cygb*-deficient mice from Figure 2 were subjected to additional biochemical and gene expression analyses. **A:** The liver was lysed and gel separated, and the levels of p-Akt, p-Erk, total Akt, total Erk, and cyclin D1 were examined by immunoblot analyses. All blots were reprobed with anti-GAPDH as a loading control. **B:** Paraffin-embedded liver sections were stained for phosphorylated Erk. Scale bar = 100 μm. **C** and **D:** Relative mRNA levels of Jun and Fos (**C**) and IL-6, Tnfα, IL-1β, and Tgfβ3 (**D**) in the nontumor (NT; n = 7 to 12) and tumor (T; n = 3 to 5) areas of the liver were determined by RT-qPCR and normalized to GAPDH. $Cygb^{+/+}$ (white bars), $Cygb^{+/-}$ (gray bars), and $Cygb^{-/-}$ (black bars) mice. Values are given as the mean ± SD of all experiments. $^{*}P < 0.05$, $^{**}P < 0.01$, and $^{***}P < 0.001$.

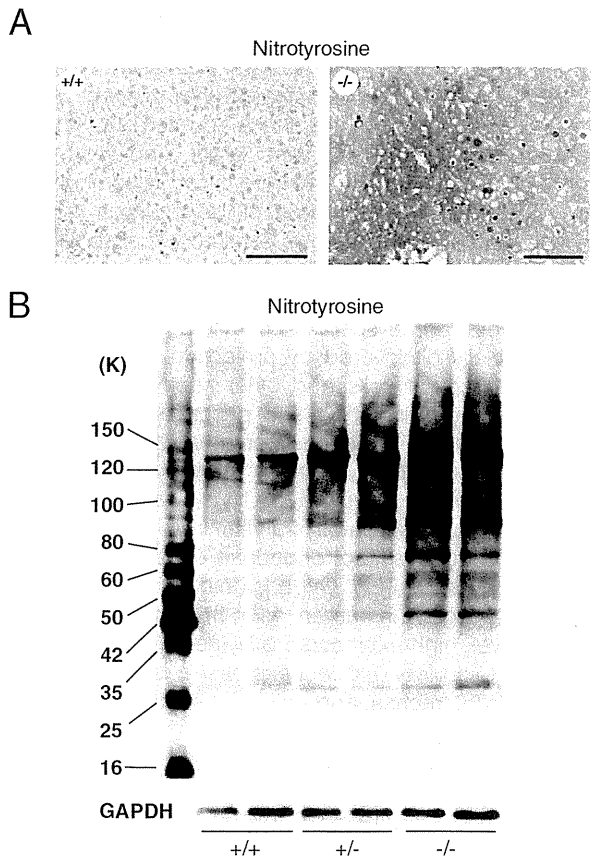

Figure 7. Peroxynitrite formation in the livers of *Cygb*-deficient mice. **A:** Paraffin-embedded liver sections from wild-type (+/+) and homozygous (−/−) mice treated with 25-ppm DEN for 25 weeks were stained with antinitrotyrosine. Nitrotyrosine-containing proteins were strongly expressed in the cytoplasm and nuclei of cancer cells in the tumor area, particularly in the inclusions of cancer cells. Scale bar = 100 μm. **B:** Protein homogenates of liver tissues from $Cygb^{+/+}$, $Cygb^{+/-}$, and $Cygb^{-/-}$ mice treated with 25-ppm DEN for 25 weeks were subjected to immunoblot detection for nitrotyrosine. GAPDH was used as a loading control. K, kDa (molecular mass).

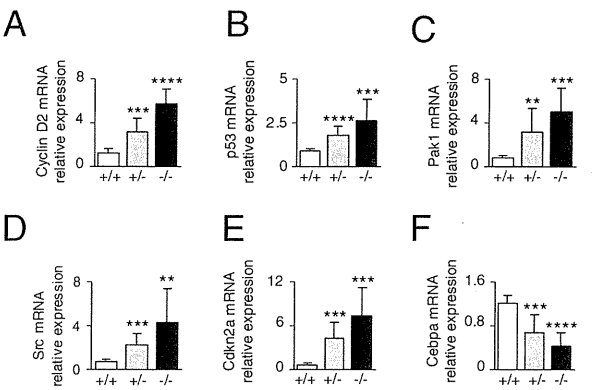

Figure 8. Altered regulation of cancer genes in *Cygb*-deficient mice. RT-qPCR analysis of cell growth–related gene transcripts cyclin D2 (**A**), p53 (**B**), and Pak1 (**C**) and cell differentiation and apoptosis-related gene transcripts Src (**D**), Cdkn2a (**E**), and Cebpa (**F**) in liver from mice treated with 25-ppm DEN for 25 weeks (n = 7 to 12). Levels are normalized to GAPDH. $Cygb^{+/+}$ (white bars), $Cygb^{+/-}$ (gray bars), and $Cygb^{-/-}$ (black bars) mice. Values are given as the mean ± SD of all experiments. $^{**}P < 0.01$, $^{***}P < 0.001$, and $^{****}P < 0.0001$.

Discussion

In the present study, we showed that loss of *Cygb* in C57BL/6J mice markedly increased their susceptibility to DEN-induced tumorigenesis. In the absence of *Cygb*, liver tumors developed earlier, were larger, and were more numerous compared with wild-type mice. By administering low-dose DEN to adult mice (0.05 ppm), which failed to induce liver cancer in wild-type mice, we observed the tumor-promoting effects of *Cygb* deficiency.

We observed high levels of Cygb expression in hepatic stellate cells, a liver-specific pericyte, from which Cygb was originally discovered by proteomic analysis of primary cultured rat cells and other stromal cells in the visceral organs, including the pancreas, gut, spleen, lung, and kidney.[1,4] These stromal cells are pericytes localized around the capillaries of the organs that are capable of vitamin A storage. Thus, we propose that Cygb may be an indicator of a vitamin A–storing phenotype of myofibroblasts of endoderm origin. However, as previously reported,[1,4,5] Cygb is ubiquitously expressed in all body organs in human, as in mice and rats. At the mRNA level, high expression is evident in the adult human heart and liver; modest expression is evident in the brain, kidney, trachea, and placenta; and low expression is evident in the adult skeletal muscle.[44] Several cancer cell lines, including HepG2 cells,[44] the NCI-H2228 lung cancer cell line, and HCC 1569 breast cancer cells,[19] also display CYGB mRNA expression. These observations indicate the role of Cygb in the regulation of cellular function originating from the epithelia. In this context, cancer development in the liver and lungs in $Cygb^{-/-}$ mice is anticipated. However, the role of mesenchymal cells that express Cygb highly in tumor development should be further evaluated because these myofibroblasts represent important environmental factors during tumor formation.

Cygb expression is augmented under hypoxia in the liver, heart, brain, and skeletal muscle and in HN33 cells (an immortalized mouse hippocampal cell line), BEAS-2B cells (a transformed human bronchial epithelial cell line), and HeLa cells (a human cervix carcinoma cell line).[16] Overexpression of Cygb protects mouse neuroblastoma N2a cells and human neuroblastoma SH-SY5Y cells under H_2O_2 exposure and the human neuronal cell line TE671 under prooxidant Ro19-8022 stimulation.[11,12,44] Overexpression of Cygb in the liver, induced by adeno-associated–virus-induced transfection, protects the liver from oxidative injury.[13] Conversely, the role of Cygb as an NO scavenger in rat hepatocytes and NIH3T3 fibroblasts may protect cells from NO-induced toxicity.[8,33] These reports and our findings regarding the accumulation of nitrotyrosine protein adducts in *Cygb*-deficient mice indicate the cytoprotective and antioxidative properties of Cygb.

Several tumor suppressor genes are located in both arms of chromosome 17. *TP53*, a known tumor suppressor gene at 17p13.1, is one of the most frequently mutated genes in cancers, including hepatocellular carcinoma.[45] *BRCA1* (breast cancer 1, early onset) at 17q12 is a human tumor suppressor gene encoding the breast cancer type 1 susceptibility protein,[46] which is present in the breast and other tissues, aiding the repair of damaged DNA and the destruction of the cell when DNA cannot be repaired. If *BRCA1* is damaged, cells duplicate uncontrollably, leading to cancer. Other known breast cancer–associated genes include *septin*, *DMC1*, and *HER2/ErbB2*.[47,48] Because *CYGB* exists on chromosome 17q25, genes on this chromosome appear commonly in the tumorigenesis of epithelial cells and mutation or epigenetic modification of these genes appears to trigger malignant transformation.

Clinically, liver cancer develops from a fibrotic liver, with chronic trauma induced by alcohol abuse and hepatitis virus B/C infection.[49] Chronic inflammation offers an appropriate environment for cancer development, by producing multiple growth factors, extracellular matrices, and neovascularization involving local hypoxia.[50] In this context, the augmented occurrence of pericellular fibrosis and fibrotic reactions (Figure 4, C–E) in *Cygb* deficiency may be involved in the development of liver cancer.

In conclusion, to our knowledge, this is the first report that *Cygb* deficiency induces susceptibility to cancer development in the liver and lungs of mice receiving DEN treatment. Thus, *Cygb*-deficient mice may provide a useful animal model to study cancer development in the liver and lungs; globins, such as Cygb, may shed new light on the biological features of organ carcinogenesis.

Acknowledgment

We thank Drs. Masaru Enomoto, Hideki Fujii, and Thoru Komiya for their valuable comments during this study.

References

1. Kawada N, Kristensen DB, Asahina K, Nakatani K, Minamiyama Y, Seki S, Yoshizato K: Characterization of a stellate cell activation-associated protein (STAP) with peroxidase activity found in rat hepatic stellate cells. J Biol Chem 2001, 276:25318–25323
2. Burmester T, Ebner B, Weich B, Hankeln T: Cytoglobin: a novel globin type ubiquitously expressed in vertebrate tissues. Mol Biol Evol 2002, 19:416–421
3. Sawai H, Kawada N, Yoshizato K, Nakajima H, Aono S, Shiro Y: Characterization of the heme environmental structure of cytoglobin, a fourth globin in humans. Biochemistry 2003, 42:5133–5142
4. Nakatani K, Okuyama H, Shimahara Y, Saeki S, Kim DH, Nakajima Y, Seki S, Kawada N, Yoshizato K: Cytoglobin/STAP, its unique localization in splanchnic fibroblast-like cells and function in organ fibrogenesis. Lab Invest 2004, 84:91–101
5. Shigematsu A, Adachi Y, Matsubara J, Mukaide H, Koike-Kiriyama N, Minamino K, Shi M, Yanai S, Imamura M, Taketani S, Ikehara S: Analyses of expression of cytoglobin by immunohistochemical studies in human tissues. Hemoglobin 2008, 32:287–296
6. Sugimoto H, Makino M, Sawai H, Kawada N, Yoshizato K, Shiro Y: Structural basis of human cytoglobin for ligand binding. J Mol Biol 2004, 339:873–885
7. Li RC, Lee SK, Pouranfar F, Brittian KR, Clair HB, Row BW, Wang Y, Gozal D: Hypoxia differentially regulates the expression of neuroglobin and cytoglobin in rat brain. Brain Res 2006, 1096:173–179
8. Fordel E, Geuens E, Dewilde S, Rottiers P, Carmeliet P, Grooten J, Moens L: Cytoglobin expression is upregulated in all tissues upon hypoxia: an in vitro and in vivo study by quantitative real-time PCR. Biochem Biophys Res Commun 2004, 319:342–348
9. Guo X, Philipsen S, Tan-Un KC: Study of the hypoxia-dependent regulation of human CYGB gene. Biochem Biophys Res Commun 2007, 364:145–150

10. Hodges NJ, Innocent N, Dhanda S, Graham M: Cellular protection from oxidative DNA damage by over-expression of the novel globin cytoglobin in vitro. Mutagenesis 2008, 23:293–298
11. Fordel E, Thijs L, Martinet W, Lenjou M, Laufs T, Van Bockstaele D, Moens L, Dewilde S: Neuroglobin and cytoglobin overexpression protects human SH-SY5Y neuroblastoma cells against oxidative stress-induced cell death. Neurosci Lett 2006, 410:146–151
12. Fordel E, Thijs L, Martinet W, Schrijvers D, Moens L, Dewilde S: Anoxia or oxygen and glucose deprivation in SH-SY5Y cells: a step closer to the unraveling of neuroglobin and cytoglobin functions. Gene 2007, 398:114–122
13. Xu R, Harrison PM, Chen M, Li L, Tsui TY, Fung PC, Cheung PT, Wang G, Li H, Diao Y, Krissansen GW, Xu S, Farzaneh F: Cytoglobin overexpression protects against damage-induced fibrosis. Mol Ther 2006, 13:1093–1100
14. McRonald FE, Liloglou T, Xinarianos G, Hill L, Rowbottom L, Langan JE, Ellis A, Shaw JM, Field JK, Risk JM: Down-regulation of the cytoglobin gene, located on 17q25, in tylosis with oesophageal cancer (TOC): evidence for trans-allele repression. Hum Mol Genet 2006, 15:1271–1277
15. Xinarianos G, McRonald FE, Risk JM, Bowers NL, Nikolaidis G, Field JK, Liloglou T: Frequent genetic and epigenetic abnormalities contribute to the deregulation of cytoglobin in non-small cell lung cancer. Hum Mol Genet 2006, 15:2038–2044
16. Shaw RJ, Omar MM, Rokadiya S, Kogera FA, Lowe D, Hall GL, Woolgar JA, Homer J, Liloglou T, Field JK, Risk JM: Cytoglobin is upregulated by tumour hypoxia and silenced by promoter hypermethylation in head and neck cancer. Br J Cancer 2009, 101: 139–144
17. Presneau N, Dewar K, Forgetta V, Provencher D, Mes-Masson AM, Tonin PN: Loss of heterozygosity and transcriptome analyses of a 1.2 Mb candidate ovarian cancer tumor suppressor locus region at 17q25.1-q25.2. Mol Carcinog 2005, 43:141–154
18. Chua PJ, Yip GW, Bay BH: Cell cycle arrest induced by hydrogen peroxide is associated with modulation of oxidative stress related genes in breast cancer cells. Exp Biol Med (Maywood) 2009, 234: 1086–1094
19. Shivapurkar N, Stastny V, Okumura N, Girard L, Xie Y, Prinsen C, Thunnissen FB, Wistuba II, Czerniak B, Frenkel E, Roth JA, Liloglou T, Xinarianos G, Field JK, Minna JD, Gazdar AF: Cytoglobin, the newest member of the globin family, functions as a tumor suppressor gene. Cancer Res 2008, 68:7448–7456
20. Sinal CJ, Tohkin M, Miyata M, Ward JM, Lambert G, Gonzalez FJ: Targeted disruption of the nuclear receptor FXR/BAR impairs bile acid and lipid homeostasis. Cell 2000, 102:731–744
21. Verna L, Whysner J, Williams GM: N-nitrosodiethylamine mechanistic data and risk assessment: bioactivation, DNA-adduct formation, mutagenicity, and tumor initiation. Pharmacol Ther 1996, 71:57–81
22. Diwan BA, Rice JM, Ohshima M, Ward JM: Interstrain differences in susceptibility to liver carcinogenesis initiated by N-nitrosodiethylamine and its promotion by phenobarbital in C57BL/6NCr, C3H/HeNCrMTV- and DBA/2NCr mice. Carcinogenesis 1986, 7:215–220
23. Drinkwater NR, Ginsler JJ: Genetic control of hepatocarcinogenesis in C57BL/6J and C3H/HeJ inbred mice. Carcinogenesis 1986, 7:1701–1707
24. Vesselinovitch SD, Koka M, Mihailovich N, Rao KV: Carcinogenicity of diethylnitrosamine in newborn, infant, and adult mice. J Cancer Res Clin Oncol 1984, 108:60–65
25. Gray R, Peto R, Brantom P, Grasso P: Chronic nitrosamine ingestion in 1040 rodents: the effect of the choice of nitrosamine, the species studied, and the age of starting exposure. Cancer Res 1991, 51: 6470–6491
26. Ward JM, Diwan BA, Ohshima M, Hu H, Schuller HM, Rice JM: Tumor-initiating and promoting activities of di(2-ethylhexyl) phthalate in vivo and in vitro. Environ Health Perspect 1986, 65:279–291
27. Iwai S, Murai T, Makino S, Min W, Morimura K, Mori S, Hagihara A, Seki S, Fukushima S: High sensitivity of fatty liver Shionogi (FLS) mice to diethylnitrosamine hepatocarcinogenesis: comparison to C3H and C57 mice. Cancer Lett 2007, 246:115–121
28. Koen H, Pugh TD, Goldfarb S: Hepatocarcinogenesis in the mouse: combined morphologic-stereologic studies. Am J Pathol 1983, 112: 89–100
29. Koen H, Pugh TD, Nychka D, Goldfarb S: Presence of alpha-fetoprotein-positive cells in hepatocellular foci and microcarcinomas induced by single injections of diethylnitrosamine in infant mice. Cancer Res 1983, 43:702–708
30. Whittaker S, Marais R, Zhu AX: The role of signaling pathways in the development and treatment of hepatocellular carcinoma. Oncogene 2010, 29:4989–5005
31. Grivennikov SI, Greten FR, Karin M: Immunity, inflammation, and cancer. Cell 2010, 140:883–899
32. Kamimura D, Ishihara K, Hirano T: IL-6 signal transduction and its physiological roles: the signal orchestration model. Rev Physiol Biochem Pharmacol 2003, 149:1–38
33. Ahn B, Han BS, Kim DJ, Ohshima H: Immunohistochemical localization of inducible nitric oxide synthase and 3-nitrotyrosine in rat liver tumors induced by N-nitrosodiethylamine. Carcinogenesis 1999, 20: 1337–1344
34. Kheirollahi M, Mehr-Azin M, Kamalian N, Mehdipour P: Expression of cyclin D2, P53, Rb and ATM cell cycle genes in brain tumors. Med Oncol 2011, 28:7–14
35. Kumar R, Gururaj AE, Barnes CJ: p21-activated kinases in cancer. Nat Rev Cancer 2006, 6:459–471
36. Siu MK, Wong ES, Chan HY, Kong DS, Woo NW, Tam KF, Ngan HY, Chan QK, Chan DC, Chan KY, Cheung AN: Differential expression and phosphorylation of Pak1 and Pak2 in ovarian cancer: effects on prognosis and cell invasion. Int J Cancer 2010, 127:21–31
37. Barnekow A, Paul E, Schartl M: Expression of the c-src proto-oncogene in human skin tumors. Cancer Res 1987, 47:235–240
38. McClain KL: Expression of oncogenes in human leukemias. Cancer Res 1984, 44:5382–5389
39. Maelandsmo GM, Berner JM, Florenes VA, Forus A, Hovig E, Fodstad O, Myklebost O: Homozygous deletion frequency and expression levels of the CDKN2 gene in human sarcomas: relationship to amplification and mRNA levels of CDK4 and CCND1. Br J Cancer 1995, 72:393–398
40. Belinsky SA, Swafford DS, Middleton SK, Kennedy CH, Tesfaigzi J: Deletion and differential expression of p16INK4a in mouse lung tumors. Carcinogenesis 1997, 18:115–120
41. Timchenko NA, Wilde M, Nakanishi M, Smith JR, Darlington GJ: CCAAT/enhancer-binding protein alpha (C/EBP alpha) inhibits cell proliferation through the p21 (WAF-1/CIP-1/SDI-1) protein. Genes Dev 1996, 10:804–815
42. Diehl AM, Johns DC, Yang S, Lin H, Yin M, Matelis LA, Lawrence JH: Adenovirus-mediated transfer of CCAAT/enhancer-binding protein-alpha identifies a dominant anti-proliferative role for this isoform in hepatocytes. J Biol Chem 1996, 271:7343–7350
43. Pabst T, Mueller BU, Harakawa N, Schoch C, Haferlach T, Behre G, Hiddemann W, Zhang DE, Tenen DG: AML1-ETO downregulates the granulocytic differentiation factor C/EBPalpha in t(8;21) myeloid leukemia. Nat Med 2001, 7:444–451
44. Asahina K, Kawada N, Kristensen DB, Nakatani K, Seki S, Shiokawa M, Tateno C, Obara M, Yoshizato K: Characterization of human stellate cell activation-associated protein and its expression in human liver. Biochem Biophys Acta 2002, 1577:471–475
45. Caron de Fromentel C, Soussi T: TP53 tumor suppressor gene: a model for investigating human mutagenesis. Genes Chromosomes Cancer 1992, 4:1–15
46. Deng CX: BRCA1: cell cycle checkpoint, genetic instability, DNA damage response and cancer evolution. Nucleic Acids Res 2006, 34:1416–1426
47. Harada H, Nagai H, Tsuneizumi M, Mikami I, Sugano S, Emi M: Identification of DMC1, a novel gene in the TOC region on 17q25.1 that shows loss of expression in multiple human cancers. J Hum Genet 2001, 46:90–95
48. Coussens L, Yang-Feng TL, Liao YC, Chen E, Gray A, McGrath J, Seeburg PH, Libermann TA, Schlessinger J, Francke U, Levinson A, Ullrich A: Tyrosine kinase receptor with extensive homology to EGF receptor shares chromosomal location with neu oncogene. Science 1985, 230:1132–1139
49. Llovet JM, Burroughs A, Bruix J: Hepatocellular carcinoma. Lancet 2003, 362:1907–1917
50. Brunt EM: Pathology of nonalcoholic fatty liver disease. Nat Rev Gastroenterol Hepatol 2010, 7:195–203

Rapid Emergence of Telaprevir Resistant Hepatitis C Virus Strain from Wildtype Clone *In Vivo*

Nobuhiko Hiraga,[1,2] Michio Imamura,[1,2] Hiromi Abe,[1,2] C. Nelson Hayes,[1,2] Tomohiko Kono,[1,2] Mayu Onishi,[1,2] Masataka Tsuge,[1,2] Shoichi Takahashi,[1,2] Hidenori Ochi,[2,3] Eiji Iwao,[4] Naohiro Kamiya,[4] Ichimaro Yamada,[4] Chise Tateno,[2,5] Katsutoshi Yoshizato,[2,5] Hirotaka Matsui,[6] Akinori Kanai,[7] Toshiya Inaba,[6] Shinji Tanaka,[1,2] and Kazuaki Chayama[1,2,3]

Telaprevir is a potent inhibitor of hepatitis C virus (HCV) NS3-4A protease. However, the emergence of drug-resistant strains during therapy is a serious problem, and the susceptibility of resistant strains to interferon (IFN), as well as the details of the emergence of mutant strains *in vivo*, is not known. We previously established an infectious model of HCV using human hepatocyte chimeric mice. Using this system we investigated the biological properties and mode of emergence of mutants by ultra-deep sequencing technology. Chimeric mice were injected with serum samples obtained from a patient who had developed viral breakthrough during telaprevir monotherapy with strong selection for resistance mutations (A156F [92.6%]). Mice infected with the resistant strain (A156F [99.9%]) developed only low-level viremia and the virus was successfully eliminated with interferon therapy. As observed in patients, telaprevir monotherapy in viremic mice resulted in breakthrough, with selection for mutations that confer resistance to telaprevir (e.g., a high frequency of V36A [52.2%]). Mice were injected intrahepatically with HCV genotype 1b clone KT-9 with or without an introduced resistance mutation, A156S, in the NS3 region, and treated with telaprevir. Mice infected with the A156S strain developed lower-level viremia compared to the wildtype strain but showed strong resistance to telaprevir treatment. Although mice injected with wildtype HCV showed a rapid decline in viremia at the beginning of therapy, a high frequency (11%) of telaprevir-resistant NS3 V36A variants emerged 2 weeks after the start of treatment. *Conclusion:* Using deep sequencing technology and a genetically engineered HCV infection system, we showed that the rapid emergence of telaprevir-resistant HCV was induced by mutation from the wildtype strain of HCV *in vivo*. (HEPATOLOGY 2011;54:781-788)

Chronic hepatitis C virus (HCV) infection is a leading cause of cirrhosis, liver failure, and hepatocellular carcinoma.[1,2] The current standard treatment for patients chronically infected with HCV is the combination of peg-interferon (PEG-IFN) and ribavirin (RBV).[3-5] However, this treatment results in sustained viral response (SVR), defined as negative for HCV RNA 24 weeks after cessation of the therapy, in only about 50% of patients with genotype 1 HCV infection with high viral loads.[3-5] Given the low

Abbreviations: HCV, hepatitis C virus; HSA, human serum albumin; PEG-IFN, peg-interferon; RBV, ribavirin; RT-PCR, reverse transcript-polymerase chain reaction; SCID, severe combined immunodeficiency; SVR, sustained viral response; uPA, urokinase-type plasminogen activator.

From the [1]Department of Medicine and Molecular Science, Division of Frontier Medical Science, Programs for Biomedical Research, Graduate School of Biomedical Sciences, Hiroshima University, Hiroshima, Japan; [2]Liver Research Project Center, Hiroshima University, Hiroshima, Japan; [3]Laboratory for Digestive Diseases, RIKEN Center for Genomic Medicine, Hiroshima, Japan; [4]Research and Development Unit, Mitsubishi Tanabe Pharma Corp., Yokohama, Japan; [5]PhoenixBio Co., Ltd., Higashihiroshima, Japan; [6]Department of Molecular Oncology and Leukemia Program Project, Research Institute for Radiation Biology and Medicine, Hiroshima University, Hiroshima, Japan; [7]Radiation Research Center for Frontier Science, Research Institute for Radiation Biology and Medicine, Hiroshima University, Hiroshima, Japan.

Received January 17, 2011; accepted May 16, 2011.

Supported in part by a grant-in-aid for Scientific Research from the Japanese Ministry of Labor, Health and Welfare

Address reprint requests to: Prof. Kazuaki Chayama, M.D., Ph.D., Department of Medical and Molecular Science, Division of Frontier Medical Science, Programs for Biomedical Research, Graduate School of Biomedical Science, Hiroshima University, 1-2-3 Kasumi, Minami-ku, Hiroshima 734-8551, Japan. E-mail: chayama@hiroshima-u.ac.jp; fax: +81-82-255-6220.

View this article online at wileyonlinelibrary.com.

DOI 10.1002/hep.24460

Potential conflict of interest: E.I., N.K., I.Y. are employees of Mitsubishi Tanabe Pharma Corp. The other authors have nothing to declare.

effectiveness of the current therapy, many molecules have been screened for antiviral activity against HCV for use in development of novel anti-HCV therapies. A number of new selective inhibitors of HCV proteins, the so-called STAT-C (specifically targeted antiviral therapy for HCV) inhibitors, are currently under development. Telaprevir is a reversible, selective, specific inhibitor of the HCV NS3-4A protease that has shown potent antiviral activity in HCV replicon assays.[6] Although the antiviral effect of telaprevir is quite potent, monotherapy using these drugs results in rapid emergence of drug-resistant strains.[7,8] Accordingly, these drugs are used in combination with pegylated-IFN and ribavirin for chronic hepatitis C patients. Because the HCV virus replicates rapidly and RNA polymerase lacks a proofreading system, HCV viral quasispecies can emerge *de novo*, and some of these variants may confer resistance. Although a resistant variant is initially present at low frequency, it may quickly emerge as the dominant species during antiviral treatment.[9,10] Resistant clones against HCV NS3-4A protease inhibitors have reportedly been induced in replicon systems.

The immunodeficient urokinase-type plasminogen activator (uPA) mouse permits repopulation of the liver with human hepatocytes, resulting in human hepatocyte chimeric mice that are able to develop HCV viremia after injection of serum samples positive for the virus.[11] We and other groups have reported that the human hepatocyte chimeric mouse is useful for evaluating the effect of NS3-4A protease inhibitor.[12,13] Using this mouse model, we developed a reverse genetics systems for HCV.[14,15] This system is useful to study characteristics of HCV strains with various substitutions of interest because the confounding effects of quasispecies can be minimized. Using ultra-deep sequencing technology, we demonstrate the rapid emergence of telaprevir resistance in HCV as a result of mutation from wildtype strain using genetically engineered HCV-infected human hepatocyte chimeric mice.

Materials and Methods

Animal Treatment. Generation of the uPA$^{+/+}$/SCID$^{+/+}$ mice and transplantation of human hepatocytes were performed as described recently by our group.[16] All mice were transplanted with frozen human hepatocytes obtained from the same donor. Mice received humane care and all animal protocols were performed in accordance with the guidelines of the local committee for animal experiments. Infection, extraction of serum samples, and sacrifice were performed under ether anesthesia. Mice were injected either intravenously with HCV-positive human serum samples or intrahepatically with *in vitro*-transcribed genotype 1b HCV RNA. HCV-infected mice were administered either perorally with 200-300 mg/kg of telaprevir (VX950; MP424; Mitsubishi Tanabe Pharma, Osaka, Japan) twice a day or intramuscularly with 1,500 IU/g of IFN-alpha (Dainippon Sumitomo Pharma, Tokyo). The telaprevir dose was determined in a previous study in which this dosage range was found to yield serum concentrations equivalent to treated human patients.[13]

Human Serum Samples. After obtaining written informed consent, human serum samples containing genotype 1b HCV were obtained from two patients with chronic hepatitis. The individual serum samples were divided into aliquots and stored separately in liquid nitrogen until use. The study protocol conforms to the ethical guidelines of the 1975 Declaration of Helsinki and was approved *a priori* by the Institutional Review Committee.

HCV RNA Transcription and Inoculation into Chimeric Mice. We have previously established an infectious genotype 1b HCV clone HCV-KT9 derived from a Japanese patient with severe acute hepatitis (GenBank access. no. AB435162).[15] We cloned this HCV complementary DNA (cDNA) into plasmid pBR322 under a T7 RNA promoter to create the plasmid pHCV-KT9. Ten μg of plasmid DNA, linearized by *Xba*I (Promega, Madison, WI) digestion, were transcribed in a 100 μL reaction volume with T7 RNA polymerase (Promega) at 37°C for 2 hours and analyzed by agarose gel electrophoresis. Each transcription mixture was diluted with 400 μL of phosphate-buffered saline (PBS) and injected into the livers of chimeric mice.[15] The QuikChange site-directed mutagenesis kit (Stratagene, Foster City, CA) was used to introduce a substitution at amino acid 156 of the NS3 region (A156S).

RNA Extraction and Amplification. RNA was extracted from serum samples by Sepa Gene RV-R (Sankojunyaku, Tokyo), dissolved in 8.8 μL RNase-free H_2O, and reverse transcribed using a random primer (Takara Bio, Shiga, Japan) and M-MLV reverse transcriptase (ReverTra Ace, Toyobo, Osaka, Japan) in a 20-μL reaction mixture according to the instructions provided by the manufacturer. Nested polymerase chain reaction (PCR) and quantitation of HCV by Light Cycler (Roche Diagnostic, Japan, Tokyo) were performed as reported.[15]

Ultra-Deep Sequencing. We adapted multiplex sequencing-by-synthesis to simultaneously sequence

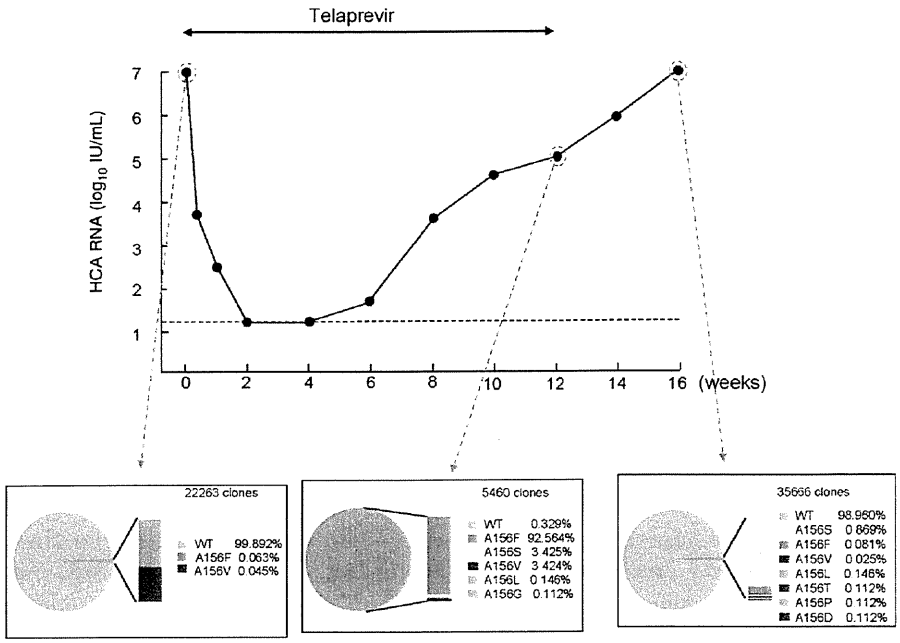

Fig. 1. Changes in serum HCV RNA levels in a telaprevir-treated chronic hepatitis C patient. A 55-year-old woman infected with genotype 1b HCV was treated with 750 mg of telaprevir every 8 hours for 12 weeks. Serum HCV RNA (upper panel) and the amino acid (aa) frequencies at aa156 in the HCV NS3 region by ultra-deep sequencing at the indicated times are shown. The horizontal dotted line indicates the detectable limit (1.2 log copy/mL).

multiple genomes using the Illumina Genome Analyzer. Briefly, cDNA was fragmented using sonication and the resultant fragment distribution was assessed using the Agilent BioAnalyzer 2100 platform. A library was prepared using the Multiplexing Sample Preparation Kit (Illumina, CA). Imaging analysis and base calling were performed using Illumina Pipeline software with default settings.[17-23] The N-terminal 543 nucleotides of NS3 protease were analyzed. This technique revealed an average coverage depth of over 1,000 sequence reads per basepair in the unique regions of the genome. Read mapping to a reference sequence was performed using Bowtie.[24] Because of the short 36 nucleotide read length, mapping hypervariable regions with multiple closely spaced variants against a reference sequence yields poor coverage. Therefore, common variants were identified by relaxing the mismatch settings as well as using *de novo* assembly using ABySS.[25] Multiple alternative reference sequences were included to improve coverage in variable regions. Codon counts were merged and analyzed using R v. 2.12.

Results

Emergence of a Telaprevir-Resistant Variant in a Hepatitis C Patient Treated with Telaprevir and Analysis of the A156F Mutation. A 55-year-old woman infected with genotype 1b HCV was treated with 750 mg of telaprevir every 8 hours for 12 weeks (Fig. 1). After 1 weeks of treatment, serum HCV RNA titer decreased below the detectable limit (1.2 log copy/mL). However, HCV RNA titer became positive by week 4. By week 12, HCV RNA titer had increased to 4.8 log copy/mL and telaprevir treatment was discontinued. Because direct sequence analysis showed an A156F mutation in the NS3 region in the serum samples at 12 weeks, we performed ultra-deep sequence analysis and confirmed the high frequency (92.5%) of A156F mutation. Four weeks after cessation of treatment (at 16 weeks), sequence analysis revealed that the major strain had reverted to wildtype (99%). To analyze the replication ability and the susceptibility of the A156F mutation to telaprevir, 100 μL serum samples containing 10^4 copies of HCV obtained at week 12 were injected into human hepatocyte chimeric mice. Two wildtype HCV-inoculated mice became positive for HCV RNA 2 weeks after inoculation and serum HCV RNA titer increased to high levels (7.6 and 7.8 log copy/mL, respectively) at 6 weeks after inoculation (Fig. 2). In contrast to wildtype HCV-infected mice, a mouse inoculated with serum containing the A156F mutant developed measurable viremia at 4 weeks postinoculation, although serum HCV RNA titer remained low at 6 weeks (5.2 log copy/mL). Eight weeks after inoculation ultra-deep sequence analysis showed a high frequency (99.9%) of A156F mutation. From this point the mouse was administrated 200 mg/kg of telaprevir perorally twice a day for 4 weeks. However, this treatment resulted in no reduction in serum HCV RNA level. During the observation period the A156F mutation remained at

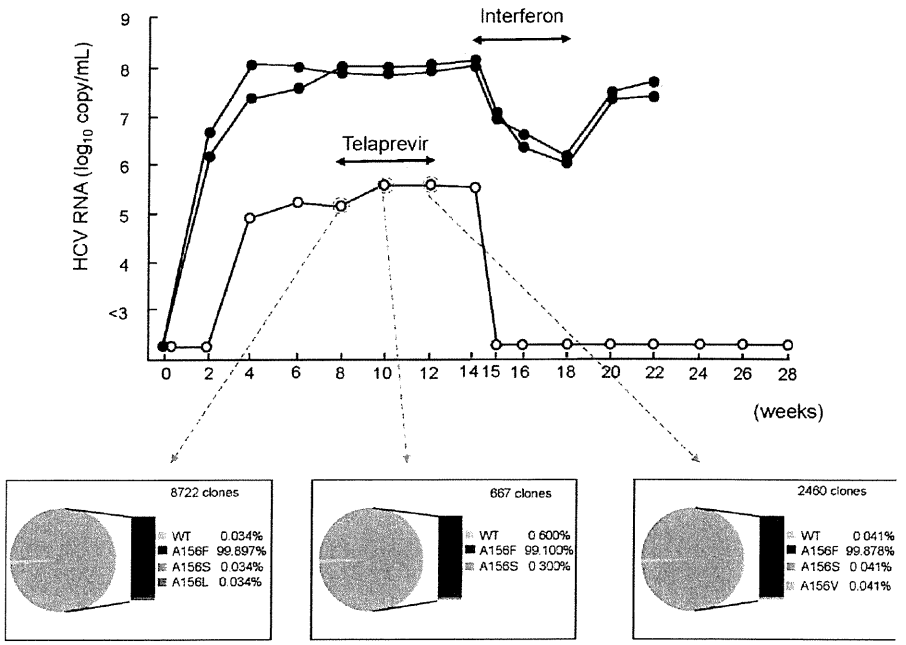

Fig. 2. Changes in serum virus titers in HCV-infected mice. Mice were injected with either wildtype (closed circles) or A156F-mutated HCV serum samples (obtained from an HCV-infected patient who received telaprevir monotherapy for 12 weeks; see Fig. 1) (open circles). Six weeks after injection the A156F mutant mouse was treated with 200 mg/kg of telaprevir orally twice a day for 4 weeks and injected intramuscularly with 1,500 IU/g/day of interferon-alpha for 4 weeks. Serum HCV RNA (upper panel) and amino acid (aa) frequencies at aa156 in the HCV NS3 region by ultra-deep sequencing at the indicated times are shown.

high frequency (>99%). To analyze the susceptibility of the A156F mutation to IFN, wildtype or A156F-mutated HCV-infected mice were treated with 1,500 IU/g/day of IFN-alpha for 4 weeks. Treatment resulted in only a two log reduction in HCV RNA level in wildtype HCV-infected mice. In contrast, serum HCV RNA titer decreased below the detectable limit 1 week after treatment in an A156F-infected mouse. Ten weeks after cessation of IFN-treatment (at week 28), HCV RNA in the mouse serum remained undetectable, suggesting that HCV RNA was eliminated. These results demonstrate that the A156F variant is associated with telaprevir-resistance, but the mutant has low replication ability and a high susceptibility to IFN.

Effect of Telaprevir on HCV-Infected Mice and Sequence Analysis of NS3 Region. Next we investigated the effect of telaprevir on wildtype HCV-infected mice. Two chimeric mice were inoculated intravenously with serum samples containing 10^5 copies of HCV obtained from an HCV-positive patient (Fig. 3). Six weeks after inoculation both mice were administered 200 mg/kg of telaprevir perorally twice a day for 4 weeks. Serum HCV RNA titer in both mice rapidly decreased; however, in one of the mice HCV RNA titer increased again 3 weeks after the start of treatment. Ultra-deep sequence analysis of the NS3 region showed that following the start of telaprevir administration the frequency of the V36A mutation increased from 18% at 2 weeks to 52% at 4 weeks, at which point it was accompanied by an increase in the HCV RNA titer. Two weeks after cessation of telaprevir treatment (at week 12), ultra-deep sequence analysis revealed that the frequency of the V36A mutant had decreased to 13% and the frequency of the wildtype HCV had increased to 84%, although the HCV RNA titer increased only slightly.

Intrahepatic Injection of HCV-KT9-Wild RNA and KT9-NS3-A156S RNA into Human Hepatocyte Chimeric Mice. We previously established an infectious genotype 1b HCV clone, HCV-KT9 (HCV-KT9-wild).[15] We created a telaprevir-resistant HCV clone by introducing an A156S amino acid substitution in the NS3 region of HCV-KT9 (KT9-NS3-A156S) (Fig. 4A). Using wildtype and telaprevir-resistant clones we investigated the replication ability *in vivo*. Mice were injected intrahepatically with 30 μg of *in vitro*-transcribed HCV-KT9-wild RNA or KT9-NS3-A156S RNA. Mice injected with HCV-KT9-wild developed measurable viremia at 2 weeks postinoculation and by 4 weeks postinoculation HCV RNA had reached 10^7 copy/mL (Fig. 4B). On the other hand, mice injected with KT9-NS3-A156S developed measurable viremia at 4 weeks postinoculation but maintained only low levels of viremia. These results suggest that the telaprevir-resistant HCV clone has a lowered replication ability compared to the wildtype HCV clone *in vivo*.

Treatment with Telaprevir and Analysis of Mutagenesis in Mice. Two mice infected with HCV-KT9-wild and one mouse infected with KT9-NS3-A156S were treated with 200 mg/kg of telaprevir twice a day for 2 weeks (Fig. 5A), resulting in 1.4 and 2.7 log

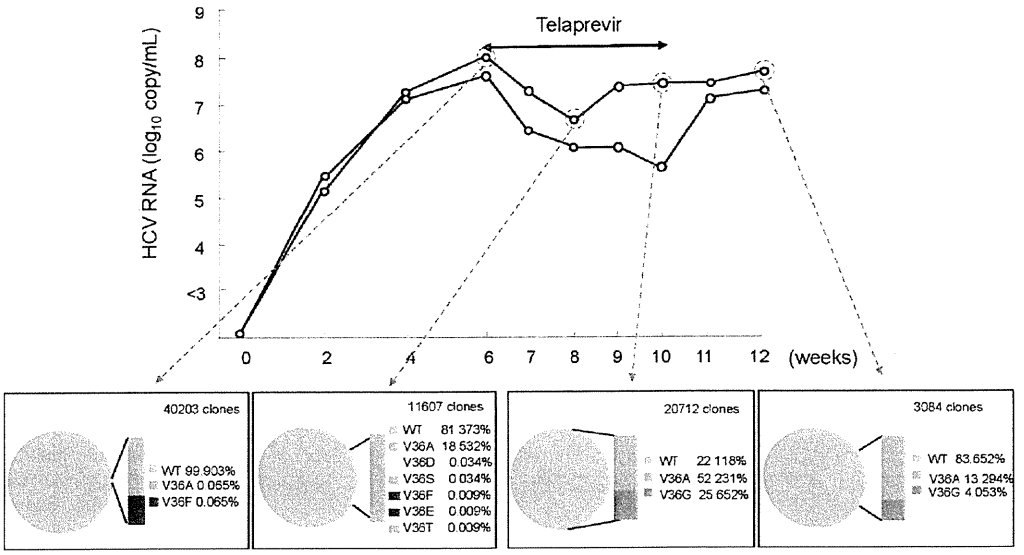

Fig. 3. Treatment with telaprevir in wildtype HCV-infected mice. Two mice were injected intravenously with 50 μL of HCV-positive human serum samples. Six weeks after HCV injection mice were treated with 200 mg/kg of telaprevir orally twice a day for 4 weeks. Serum HCV RNA (upper panel) and amino acid (aa) frequencies at aa36 in the HCV NS3 region by ultra-deep sequencing at the indicated times are shown.

reductions in HCV RNA level in the two wildtype HCV-infected mice. In contrast, only a 0.6 log reduction was observed in the KT9-NS3-A156S-infected mouse. These results demonstrate that our human hepatocyte chimeric mouse model infected with *in vitro*-transcribed HCV RNA provides an effective system for analysis of the susceptibility of HCV mutants to antiviral drugs. Interestingly, ultra-deep sequence analysis showed a rapid emergence of a V36A variant in the NS3 region in mouse serum 2 weeks after treatment (Fig. 5B). Four weeks after cessation of treatment (at week 6) the frequency of the V36A variant had decreased. Mice were then treated with 300 mg/kg of telaprevir twice a day for 4 weeks, which resulted in an elevated frequency of V36A variants at 1 (at week 7, 5.4%) and 4 weeks (at 10 week, 41.8%) after treatment and no reduction in serum HCV RNA level. These results suggest that telaprevir-resistant mutations emerged *de novo* from the wildtype strain of HCV, presumably through error-prone replication and potent selection for telaprevir escape mutants. During the telaprevir treatment period no increases of HCV RNA titers in these mice were observed, probably due to the low frequency of the resistant strain.

Discussion

Telaprevir is a peptidomimetic inhibitor of the NS3-4A serine protease that is currently undergoing clinical evaluation. Despite its effectiveness against HCV, some patients have shown a rapid viral breakthrough during the first 14 days of treatment.[26] Population sequencing of the viral NS3 region identified a number of mutations near the NS3 protease catalytic

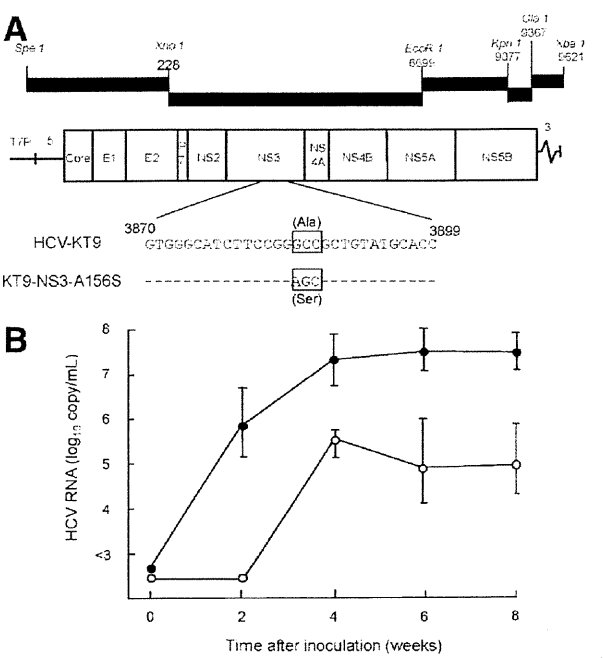

Fig. 4. Intrahepatic injection of *in vitro* transcribed HCV-KT9 RNA and KT9-NS3-A156S RNA into human hepatocyte chimeric mice. (A) The schematic of infectious genotype 1b HCV clones, HCV-KT9 and KT9-NS3-A156S. Boxes indicate codons at amino acid 156 in HCV NS3 region. Ala, alanine; Ser, serine. (B) Changes in serum levels of HCV RNA in mice intrahepatically injected with either HCV-KT9 RNA (closed circles) or KT9-NS3-A156S RNA (open circles). Data are represented as the mean ± SD of three mice.

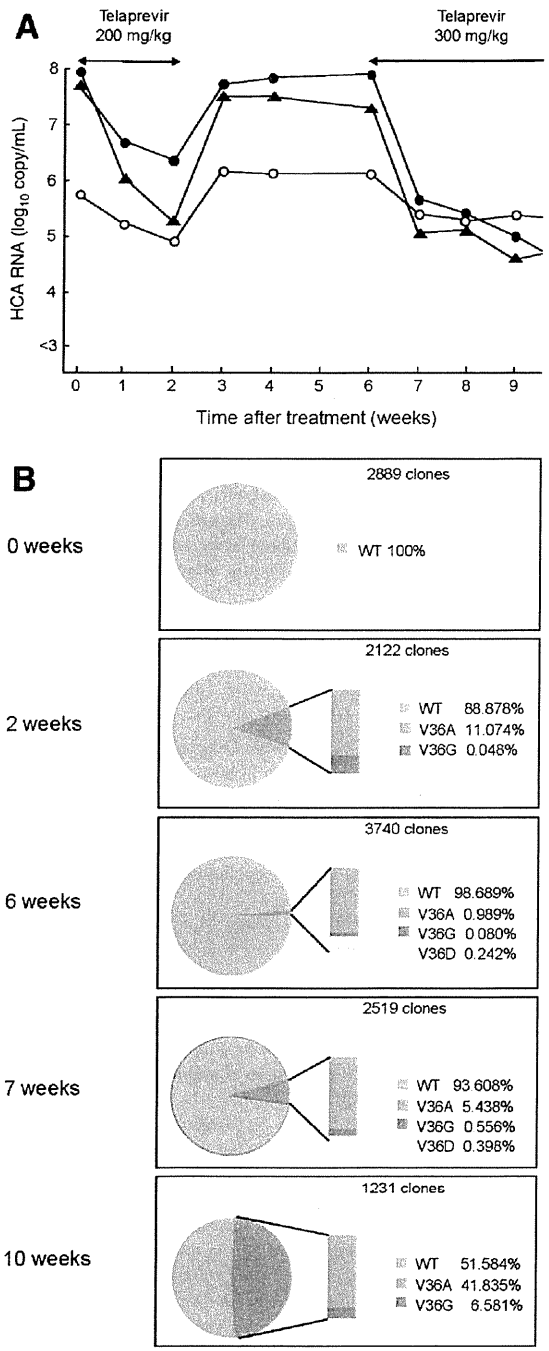

Fig. 5. The effect of telaprevir on mice infected with *in vitro*-transcribed HCV. Mice were injected with *in vitro*-transcribed HCV-KT9 RNA (closed circles and closed triangles) or KT9-NS3-A156S RNA (open circles). Six weeks after HCV RNA injection, mice were treated perorally with 200 mg/kg of telaprevir twice a day for 2 weeks. Four weeks after cessation of treatment mice were treated with 300 mg/kg of telaprevir twice a day for 4 weeks. (A) Mice serum HCV RNA titers at the indicated times are shown. Serum samples obtained from one of two HCV-KT9-infected mice (closed triangles) were used for ultra-deep sequencing. (B) Amino acid (aa) frequencies at aa36 in the HCV NS3 region based on ultra-deep sequencing are shown.

domain.[26] In particular, variants at NS3 residues 36, 54, 155, and 156 were shown to confer reduced sensitivity to telaprevir.[27]

In this study we analyzed the association between the antiviral efficacy of telaprevir and sequence variants within the NS3 region using chimeric mice infected with serum samples obtained from an HCV genotype 1b-infected patient. One of two HCV-infected mice had a viral breakthrough during the dosing period (Fig. 3). Ultra-deep sequence analysis of the NS3 region showed an increase of the V36A mutant, which has been reported to confer telaprevir resistance.[26] Consequently, our results show evidence of emergence of a telaprevir-resistant variant previously detected in human clinical trials.

We detected an A156F mutant in the HCV NS3 region in a chronic hepatitis patient who had experienced viral breakthrough during telaprevir monotherapy (Fig. 1). Likewise, HCV RNA titer in mice infected with the A156F variant showed no reduction following 2 weeks of telaprevir treatment (Fig. 2). However, 2 weeks of treatment with IFN-alpha rapidly suppressed serum HCV RNA titer below the detectable limit. These results demonstrate that A156F is telaprevir-resistant but has a high susceptibility to IFN.

Interestingly, ultra-deep sequencing revealed that the wildtype strain was present at low frequency (0.3%) in the serum inoculum (Fig. 2). However, the frequency of the wildtype failed to increase over time (Fig. 3), suggesting that the very small number of wildtype viral RNA (about 30 copies) may be incomplete or defective, as a large proportion of viral genomes are thought to be defective due to the virus's high replication and mutation rates.[9] Further analysis is necessary in order to interpret the significance of the presence of very low frequency variants detected by ultra-deep sequencing.

The short read lengths used in next generation sequencing also complicates the detection of rare variants, especially when variants are clustered within a region smaller than an individual read length (e.g., 36 basepairs). Relaxing the matching criteria allows mapping of more diverse reads but increases the error rate, whereas default settings may be geared toward more genetically homogenous haploid or diploid genomes. In this study we used *de novo* assembly to identify more diverse variants that failed to map to the reference sequence. Examining the variation in codon frequencies among samples, we created alternative reference sequences containing a sufficient range of variants to provide more uniform coverage of variable regions.

Using our previously established infectious HCV-KT9 genotype 1b HCV clone, we investigated the antiviral efficacy of telaprevir and the effect of

resistance mutations on viral replication. HCV RNA titer in mice infected with the telaprevir-resistant strain KT9-NS3-A156S was lower than in mice infected with the wildtype strain HCV-KT9-wild (Fig. 4B). HCV NS proteins include proteases for sequential processing of the polyprotein and are thought to be important in viral replication.[28] Our results suggest that differences in viral fitness underlie the differences in viral replication capacity. We analyzed the antiviral efficacy of telaprevir and the sequence of the NS3 region using HCV-infected mice treated with telaprevir. Although telaprevir treatment suppressed serum HCV RNA titer in mice infected with HCV-KT9, the decline of HCV RNA titer was only 0.6 log copy/mL in a mouse infected with KT9-NS3-A156S under the same treatment (Fig. 5A). These results suggest that our genetically engineered HCV-infected mouse model is useful for analyzing HCV escape mutants associated with antiviral drugs. Interestingly, treatment with telaprevir resulted in selection for V36A variants in the NS3 region in an HCV-KT9-infected mouse (Fig. 5B). There are a few controversial reports proposing that resistant variants may already be present at low frequency (<1%) within the quasispecies population in treatment-naïve patients,[29] consistent with their rapid emergence only days after treatment initiation.[26,30] This might well occur, due to the large number of mutated HCV clones. However, our results provide evidence in support of *de novo* emergence of telaprevir resistance induced by viral mutation followed by selection. HCV has both a high replication rate (10^{12} particles per day) and a high mutation rate (10^{-3} to 10^{-4}),[9,10] suggesting that the viral quasispecies population is likely to represent a large and genetically diverse substrate for immune selection.

In summary, we established an infection model of a genotype 1b HCV clone using the human hepatocyte chimeric mouse model. Using this model we demonstrate rapid emergence of *de novo* telaprevir-resistant HCV quasispecies from wildtype HCV.

Acknowledgment: The authors thank Rie Akiyama, Kazuyo Hattori, Yoshie Yoshida, Kiyomi Toyota, and Yoko Matsumoto for expert technical assistance.

References

1. Kiyosawa K, Sodeyama T, Tanaka E, Gibo Y, Yoshizawa K, Nakano Y, et al. Interrelationship of blood transfusion, non-A, non-B hepatitis and hepatocellular carcinoma: analysis by detection of antibody to hepatitis C virus. HEPATOLOGY 1990;12:671-675.
2. Niederau C, Lange S, Heintges T, Erhardt A, Buschkamp M, Hurter D, et al. Prognosis of chronic hepatitis C: results of a large, prospective cohort study. HEPATOLOGY 1998;28:1687-1695.
3. Manns MP, McHutchison JG, Gordon SC, Rustgi VK, Shiffman M, Reindollar R, et al. Peginterferon alfa-2b plus ribavirin compared with interferon alfa-2b plus ribavirin for initial treatment of chronic hepatitis C: a randomised trial. Lancet 2001;358:958-965.
4. Fried MW, Shiffman ML, Reddy KR, Smith C, Marinos G, Goncales FL Jr, et al. Peginterferon alfa-2a plus ribavirin for chronic hepatitis C virus infection. N Engl J Med 2002;347:975-982.
5. Hoofnagle JH, Ghany MG, Kleiner DE, Doo E, Heller T, Promrat K, et al. Maintenance therapy with ribavirin in patients with chronic hepatitis C who fail to respond to combination therapy with interferon alfa and ribavirin. HEPATOLOGY 2003;38:66-74.
6. Perni RB, Almquist SJ, Byrn RA, Chandorkar G, Chaturvedi PR, Courtney LF, et al. Preclinical profile of VX-950, a potent, selective, and orally bioavailable inhibitor of hepatitis C virus NS3–4A serine protease. Antimicrob Agents Chemother 2006;50: 899-909.
7. Lin C, Gates CA, Rao BG, Brennan DL, Fulghum JR, Luong YP, et al. In vitro studies of cross-resistance mutations against two hepatitis C virus serine protease inhibitors, VX-950 and BILN 2061. J Biol Chem 2005;280:36784-36791.
8. Mo H, Lu L, Pilot-Matias T, Pithawalla R, Mondal R, Masse S, et al. Mutations conferring resistance to a hepatitis C virus (HCV) RNA-dependent RNA polymerase inhibitor alone or in combination with an HCV serine protease inhibitor in vitro. Antimicrob Agents Chemother 2005;49:4305-4314.
9. Bartenschlager R, Lohmann V. Replication of hepatitis C virus. J Gen Virol 2000;81:1631-1648.
10. Rong L, Dahari H, Ribeiro RM, Perelson AS. Rapid emergence of protease inhibitor resistance in hepatitis C virus. Sci Transl Med 2010;2: 30ra32.
11. Mercer DF, Schiller DE, Elliott JF, Douglas DN, Hao C, Rinfret A, et al. Hepatitis C virus replication in mice with chimeric human livers. Nat Med 2001;7:927-933.
12. Kneteman NM, Weiner AJ, O'Connell J, Collett M, Gao T, Aukerman L, et al. Anti-HCV therapies in chimeric scid-Alb/uPA mice parallel outcomes in human clinical application. HEPATOLOGY 2006;43: 1346-1353.
13. Kamiya N, Iwao E, Hiraga N, Tsuge M, Imamura M, Takahashi S, et al. Practical evaluation of a mouse with chimeric human liver model for hepatitis C virus infection using an NS3–4A protease inhibitor. J Gen Virol 2010;91:1668-1677.
14. Hiraga N, Imamura M, Tsuge M, Noguchi C, Takahashi S, Iwao E, et al. Infection of human hepatocyte chimeric mouse with genetically engineered hepatitis C virus and its susceptibility to interferon. FEBS Lett 2007;581:1983-1987.
15. Kimura T, Imamura M, Hiraga N, Hatakeyama T, Miki D, Noguchi C, et al. Establishment of an infectious genotype 1b hepatitis C virus clone in human hepatocyte chimeric mice. J Gen Virol 2008;89: 2108-2113.
16. Tateno C, Yoshizane Y, Saito N, Kataoka M, Utoh R, Yamasaki C, et al. Near completely humanized liver in mice shows human-type metabolic responses to drugs. Am J Pathol 2004;165:901-912.
17. Cronn R, Liston A, Parks M, Gernandt DS, Shen R, Mockler T. Multiplex sequencing of plant chloroplast genomes using Solexa sequencing-by-synthesis technology. Nucleic Acids Res 2008;36:e122.
18. Mitsuya Y, Varghese V, Wang C, Liu TF, Holmes SP, Jayakumar P, et al. Minority human immunodeficiency virus type 1 variants in antiretroviral-naive persons with reverse transcriptase codon 215 revertant mutations. J Virol 2008;82:10747-10755.
19. Margeridon-Thermet S, Shulman NS, Ahmed A, Shahriar R, Liu T, Wang C, et al. Ultra-deep pyrosequencing of hepatitis B virus quasispecies from nucleoside and nucleotide reverse-transcriptase inhibitor (NRTI)-treated patients and NRTI-naive patients. J Infect Dis 2009; 199:1275-1285.
20. Szpara ML, Parsons L, Enquist LW. Sequence variability in clinical and laboratory isolates of herpes simplex virus 1 reveals new mutations. J Virol 2010;84:5303-5313.

21. Wright CF, Morelli MJ, Thebaud G, Knowles NJ, Herzyk P, Paton DJ, et al. Beyond the consensus: dissecting within-host viral population diversity of foot-and-mouth disease virus by using next-generation genome sequencing. J Virol 2011;85:2266-2275.
22. Verbinnen T, Van Marck H, Vandenbroucke I, Vijgen L, Claes M, Lin TI, et al. Tracking the evolution of multiple in vitro hepatitis C virus replicon variants under protease inhibitor selection pressure by 454 deep sequencing. J Virol 2010;84:11124-11133.
23. Wang GP, Sherrill-Mix SA, Chang KM, Quince C, Bushman FD. Hepatitis C virus transmission bottlenecks analyzed by deep sequencing. J Virol 2010;84:6218-6228.
24. Langmead B, Trapnell C, Pop M, Salzberg SL. Ultrafast and memory-efficient alignment of short DNA sequences to the human genome. Genome Biol 2009;10:R25.
25. Simpson JT, Wong K, Jackman SD, Schein JE, Jones SJ, Birol I. ABySS: a parallel assembler for short read sequence data. Genome Res 2009;19:1117-1123.
26. Sarrazin C, Kieffer TL, Bartels D, Hanzelka B, Muh U, Welker M, et al. Dynamic hepatitis C virus genotypic and phenotypic changes in patients treated with the protease inhibitor telaprevir. Gastroenterology 2007;132:1767-1777.
27. Kuntzen T, Timm J, Berical A, Lennon N, Berlin AM, Young SK, et al. Naturally occurring dominant resistance mutations to hepatitis C virus protease and polymerase inhibitors in treatment-naive patients. HEPATOLOGY 2008;48:1769-1778.
28. Hijikata M, Mizushima H, Tanji Y, Komoda Y, Hirowatari Y, Akagi T, et al. Proteolytic processing and membrane association of putative nonstructural proteins of hepatitis C virus. Proc Natl Acad Sci U S A 1993;90:10773-10777.
29. Lu L, Mo H, Pilot-Matias TJ, Molla A. Evolution of resistant M414T mutants among hepatitis C virus replicon cells treated with polymerase inhibitor A-782759. Antimicrob Agents Chemother 2007;51:1889-1896.
30. Kieffer TL, Sarrazin C, Miller JS, Welker MW, Forestier N, Reesink HW, et al. Telaprevir and pegylated interferon-alpha-2a inhibit wild-type and resistant genotype 1 hepatitis C virus replication in patients. HEPATOLOGY 2007;46:631-639.

Impact of Viral Amino Acid Substitutions and Host Interleukin-28B Polymorphism on Replication and Susceptibility to Interferon of Hepatitis C Virus

Nobuhiko Hiraga,[1,2] Hiromi Abe,[1,2] Michio Imamura,[1,2] Masataka Tsuge,[1,2] Shoichi Takahashi,[1,2] C. Nelson Hayes,[1,2] Hidenori Ochi,[2,3] Chise Tateno,[2,4] Katsutoshi Yoshizato,[2,4] Yusuke Nakamura,[5] Naoyuki Kamatani,[6] and Kazuaki Chayama[1,2,3]

Amino acid (aa) substitutions of core 70 and 91 and in the NS5A (nonstructural protein 5A) interferon sensitivity determining region (ISDR) as well as genetic polymorphisms in the host interleukin-28B (IL28B) locus affect the outcome of interferon (IFN)-based therapies for patients with chronic hepatitis C. The combination of these factors and the quasispecies nature of the virus complicate understanding of the underlying mechanism. Using infectious hepatitis C virus (HCV) genotype 1b clone HCV-KT9, we introduced substitutions at both core aa70 (Arg to Gln) and aa91 (Leu to Met). We also introduced four and nine ISDR aa substitutions into core mutant HCV-KT9. Using human hepatocyte chimeric mice with different IL28B genotypes, we examined the infectivity, replication ability, and susceptibility to IFN of these clones. Although aa substitutions in the ISDR significantly impaired infectivity and replication ability of the virus, core aa70 and 91 substitutions did not. The effect of IFN treatment was similar in core wild-type and mutant viruses. Interestingly, virus titer was significantly higher in mice with the favorable IL28B allele (rs8099917 TT and rs12979860 CC) in the transplanted hepatocytes than in mice with hepatocytes from rs8099917 TG and rs12979860 TT donors ($P < 0.001$). However, the effect of IFN was significantly greater, and intrahepatic expression levels of IFN-stimulated genes were significantly higher in mice with the favorable IL28B allele. *Conclusion*: Our data suggest that HCV replication levels and response to IFN are affected by human hepatocyte IL28B single-nucleotide polymorphism genotype and mutations in the ISDR. The mechanism underlying the clinically observed association of wild-type core protein in eradication-favorable host cells should be investigated further. (HEPATOLOGY 2011;54:764-771)

Chronic hepatitis C virus (HCV) infection is the leading cause of cirrhosis, liver failure, and hepatocellular carcinoma.[1,2] Interferon (IFN) is an essential component of therapy for patients with chronic HCV infection, and the most effective currently available therapy is combination therapy with pegylated (PEG)-IFN and ribavirin (RBV).[3-5] Among HCV genotypes, genotype 1 is the most resistant to

Abbreviations: aa, amino acid; GAPDH, glyceraldehyde-3-phosphate dehydrogenase; HCV, hepatitis C virus; HSA, human serum albumin; IFN, interferon; IL28B, interleukin-28B; ISDR, interferon-sensitivity–determining region; ISG, interferon-stimulated gene; MxA, myxovirus resistance protein A; NVR, nonvirological response; OAS, oligoadenylate synthetase; PBS, phosphate-buffered saline; PEG, pegylated; PKR, RNA-dependent protein kinase; RBV, ribavirin; RT-PCR, reverse-transcription polymerase chain reaction; SCID, severe combined immunodeficiency; SNP, single-nucleotide polymorphism; SVR, sustained virological response; uPA, urokinase-type plasminogen activator.

From the [1]Department of Medicine and Molecular Science, Division of Frontier Medical Science, Programs for Biomedical Research, Graduate School of Biomedical Sciences, Hiroshima University, Hiroshima, Japan; [2]Liver Research Project Center, Hiroshima University, Hiroshima, Japan; [3]Laboratory for Digestive Diseases, RIKEN Center for Genomic Medicine, Hiroshima, Japan; [4]PhoenixBio Co., Ltd., Higashi-Hiroshima, Japan; [5]Laboratory of Molecular Medicine, Human Genome Center, The Institute of Medical Science, University of Tokyo, Tokyo, Japan; and [6]Laboratory for Statistics, RIKEN Center for Genomic Medicine, Yokohama, Japan.

Received January 17, 2011; accepted May 14, 2011.

This study was supported, in part, by a Grant-in-Aid for Scientific Research from the Japanese Ministry of Labor, Health and Welfare.

Address reprint requests to: Kazuaki Chayama, M.D., Ph.D., Department of Medical and Molecular Science, Division of Frontier Medical Science, Programs for Biomedical Research, Graduate school of Biomedical Science, Hiroshima University, 1-2-3 Kasumi, Minami-ku, Hiroshima 734-8551, Japan. E-mail: chayama@hiroshima-u.ac.jp; fax: +81-82-255-6220.

View this article online at wileyonlinelibrary.com.

DOI 10.1002/hep.24453

Potential conflict of interest: Nothing to report.